

Colour-Dielectric Gauge Theory on a Transverse Lattice

S. Dalley^{*1} and B. van de Sande^{**}

**Department of Applied Mathematics and Theoretical Physics
Silver Street, Cambridge CB3 9EW, England*

***Institut Für Theoretische Physik III,
Staudstraße 7, D-91058 Erlangen, Germany*

Abstract

We investigate in some detail consequences of the effective colour-dielectric formulation of lattice gauge theory using the light-cone Hamiltonian formalism with a transverse lattice. As a quantitative test of this approach, we have performed extensive analytic and numerical calculations for 2 + 1-dimensional pure gauge theory in the large N limit. Because of Eguchi-Kawai reduction, one effectively studies a 1 + 1-dimensional gauge theory coupled to matter in the adjoint representation. We study the structure of coupling constant space for our effective potential by comparing with results available from conventional Euclidean lattice Monte Carlo simulations of this system. In particular, we calculate and measure the scaling behaviour of the entire low-lying glueball spectrum, glueball wavefunctions, string tension, asymptotic density of states, and deconfining temperature. We employ a new hybrid DLCQ/wavefunction basis in our calculations of the light-cone Hamiltonian matrix elements, along with extrapolation in Tamm-Dancoff truncation, significantly reducing numerical errors. Finally we discuss, in light of our results, what further measurements and calculations could be made in order to systematically remove lattice spacing dependence from our effective potential *a priori*.

¹From 1st April 1997 on leave at: Theory Division, CERN, CH-1211 Geneva 23, Switzerland.

1 Introduction

The least understood scale of the strong interactions is the intermediate one, between short distances described by asymptotically free QCD and the relatively long range phenomena of nuclear forces. A successful description of this intermediate region should not only include ‘global’ properties of hadrons, such as masses and decay constants, but also the wealth of accumulated experimental data on hadronic sub-structure. In addition one might hope to shed some light on the interface between gauge theory and nuclear physics. There are also many reasons why knowledge of hadron wavefunctions in a general Lorentz frame, particularly at the amplitude level, will be necessary for future progress in all aspects of particle physics. At present, no single approach to the strong interactions seems capable of this. In this paper we pursue an idea which, in principle, can address the above problems. As we will demonstrate, the colour-dielectric concept is both a natural description and, when combined with the light-cone Hamiltonian framework, a practical description of the strong interactions at intermediate scales. A number of authors have proposed the colour dielectric idea in various forms [1]–[6]² but, while the motivation was often elegant, results were usually of a qualitative nature. Our work is strongly foreshadowed by the work of Bardeen, Pearson, and Rabinovici [1] in which the ‘dielectric’ formulation of a light-cone transverse lattice gauge theory was first proposed (although the authors did not discuss it in quite those terms).

We characterise a dielectric formulation as one in which gluon fields, or rather the $SU(N)$ group elements they generate, are replaced by collective variables which represent an average over the fluctuations on short distance scales. These dielectric variables carry colour and form an effective gauge field theory with classical action minimised at zero field, meaning that colour flux is expelled from the vacuum at the classical level. The price one pays for starting with a simple vacuum structure, which may arise only for a rather low momentum cut-off on the effective theory, is that the effective action will be largely unknown and must be investigated *per se*. ‘Conservation of difficulty’ appears to have dashed one’s hopes. However, there are at least two reasons why shifting the complication from the vacuum to the action is desirable. Firstly, although most approaches to field theory place great emphasis on the calculation of vacuum energy and field condensates, neither of these are measured in experiment. Secondly, if one hopes to employ light-cone quantisation, which seems the only practical way to calculate the hadron’s wavefunction in a general Lorentz frame, then dealing with explicit vacuum structure can be rather awkward.

We choose to employ a lattice dielectric gauge theory in which the fields are N by N complex matrices M , in the adjoint representation of the gauge group, attached to links of the lattice [2].

²A review of subsequent investigations and more extensive references can be found in Ref. [7].

Because the lattice spacing in this theory should be rather large if the colour dielectric idea is to be valid, it is essentially impossible to obtain the effective action by explicitly integrating out gluons (blocking from the continuum). More realistic, but still essentially impossible, would be to introduce the dielectric fields by blocking the unitary link fields $U \in SU(N)$ of Wilson's lattice gauge theory [8]. That leaves a 'trial-and-error' approach where one tunes the coefficients of the effective action, or some truncation of it, until solutions exhibit the correct symmetries, such as Lorentz invariance. This more-or-less rules out a Euclidean path integral formulation, since one would have to do the integral (numerically) for each set of coefficients. A Hamiltonian approach is a viable alternative since most of the work goes into computing matrix elements of the Hamiltonian. This only needs to be done once for each operator appearing in the effective action. It is only the diagonalisation of the Hamiltonian, which can be performed much more rapidly, that needs to be repeated for different coefficients of the operators. In the light-cone Hamiltonian formulation [1] the continuum limit is taken in the temporal and in one spatial direction, leaving a transverse lattice. By using a light-cone Hamiltonian formulation the quantum vacuum remains as simple (modulo zero modes) as the classical vacuum.

Next we must choose a specific problem in order to test the practicality of this dielectric formulation. In this paper we postpone the introduction fermions (and hence quark structure functions) and study pure gauge theory. We look at glueballs in three spacetime dimensions at large N . The glueball problem is one of the most difficult one could imagine since it is ultra-relativistic and strongly interacting. However in *four* dimensions there is a dearth of accurate, detailed experimental or theoretical results which could be used as a benchmark. While there is an undoubted urge to contribute to the presently controversial debate on glueballs in nature, as a first calculation a more circumspect choice is appropriate. Fortunately there is a wealth of accurate information now available on glueballs for pure gauge theory in *three* dimensions from the recent Euclidean Lattice Monte Carlo (ELMC) simulations of Teper [9]. That work has shown that pure non-Abelian gauge theory behaves much the same way in three as in four dimensions: a discrete set of massive boundstates are generated by a linearly confining string-like force. Moreover, Teper has performed calculations for 2, 3, and 4 colours, allowing an extrapolation to the large N limit. The relevant expansion parameter is $1/N^2$ and observables measured at $1/N^2 = 0$ are extremely close to those measured at $1/N^2 = 1/9$. The large- N limit is convenient, though not essential, for our Light-Cone Transverse Lattice (LCTL) formulation, which becomes simpler in the limit of many colours. It enables us to implement Eguchi-Kawai reduction [10] to a $1 + 1$ -dimensional theory which does not need to be quenched or twisted so long as the vacuum is the simple dielectric one. It also allows us to make use of the extensive intuition developed for large- N theories in relation to string models. Indeed, our

formulation offers the rare possibility of describing the parton, constituent, and string behaviour of hadrons in one framework. The relationship between these pictures, each very different but equally successful, remains one of the outstanding enigmas of QCD.

We should emphasize that this is the first time that the LCTL formulation has been used in a serious quantitative study, and the expectations of the reader should be tempered accordingly. It was necessary to overcome a number of technical problems whose solutions probably have wider applicability. Our initial goal has been to explore the coupling constant space of the dielectric effective potential, which was largely ignored by Bardeen *et alii* [1] in their pioneering study. We will fix our effective potential by comparison with the the ELMC spectrum. This gives rise to predictions for other observables and it is non-trivial that a consistent picture emerges. In the light of our results, we will also discuss ways of measuring further observables to test Lorentz covariance and so fix the effective potential independently, as well as the *sine qua non* of a systematically improvable analytic renormalisation group analysis.

The outline of the paper is as follows. In the following section we describe in general terms the dielectric formulation on a Euclidean lattice, with particular reference to the large N limit. The associated light-cone Hamiltonian limit of the transverse lattice is constructed in Section 3. In Section 4 we obtain analytic and numerical solutions for glueballs, compare with Teper's data [9], and identify a scaling trajectory in coupling constant space. Section 5 addresses the string tension via winding modes. We discuss the asymptotic density of glueball states and associated finite temperature properties in Section 6 and compare with results from string theory. The conclusions in Section 7 contain discussion of some general points of principle, as well as the shortcomings of LCTL as used in this paper and their possible resolution. Appendix A contains some details of the proof of Eguchi-Kawai reduction in light-cone Hamiltonian formalism. In order to obtain the required numerical accuracy, we had to devise new methods of computation and extrapolation for light-cone Hamiltonians. These important techniques are collected in Appendices B and C since they are relevant to many parts of the paper.

Some of our preliminary results have been presented in Refs. [11].

2 Dielectric gauge theory on a Euclidean lattice

In this section we motivate the colour dielectric formulation of gauge theory in the context of a Euclidean lattice [2]. For intermediate scales, we stress that we have not derived it in detail from QCD at short distances, but view it as a starting point, similar to a sigma model for mesons. However, unlike a sigma model, or even a quark effective theory, there will be explicit colour-field degrees of freedom. The best we can do at this stage is to discuss the general form expected of the

effective potential. The details for the transverse lattice will be determined later by actually solving the theory as a function of the associated coupling constants.

2.1 Effective action

Let us consider Wilson's formulation [8] of lattice gauge theory. The principle observation is that, for large lattice spacing, the unitary link variables U have large fluctuations away from the identity and it may be just as well to replace them by some other set of variables which takes advantage of this randomness. Nielsen and Patkos [3] chose a 'block' transformation from the product of parallel transporters U along some set of lattice paths \mathcal{C}_{ab} weighted by $\rho(\mathcal{C}_{ab})$ between two points a and b of a sub-lattice

$$M(a, b) = \sum_{\{\mathcal{C}_{ab}\}} \rho(\mathcal{C}_{ab}) \prod_{\mathcal{C}_{ab}} U. \quad (1)$$

The blocked matrix link variable $M \in GL(N, C)$, since it is a linear combination of fairly random unitary variables. This blocking scheme has been investigated by operator matching using Monte Carlo and Schwinger-Dyson techniques [7] for $SU(2)$, with conclusions for the general form of the effective potential similar to those described below for large N . Although we will not use the reasoning (1) directly, it motivates us to search for an effective lattice gauge theory in terms of such non-compact link variables.

One knows that at large lattice spacing a Wilson's action gives a fair description of non-Abelian physics. One assumes that as $a \rightarrow 0$ the lattice errors gradually reduce to nil. In order to reduce the lattice errors at a finite a one might imagine 'smearing' the link variables U . Therefore consider introducing both a unitary matrix $U(l)$ and a complex matrix $M(l)$ on each link l of the spacetime lattice, with partition function

$$Z = \int \prod_l \mathcal{D}U(l) \mathcal{D}M(l) \exp \left(\frac{1}{g_L^2} \sum_P \text{Tr}_P[M] - \frac{N}{\lambda} \sum_l \text{Tr} \{ (M(l) - U(l))(M^\dagger(l) - U^\dagger(l)) \} \right) \quad (2)$$

where $\text{Tr}_P[M]$ denotes the trace of the product of link variables M around an elementary plaquette P and g_L is the dimensionless lattice gauge coupling constant. \mathcal{D} denotes the usual Haar measure, which is simply

$$\mathcal{D}M = \prod_{i,j=1}^N dM_{ij} dM_{ij}^* \quad (3)$$

for the complex matrices. In this case we have introduced a simple Gaussian smearing function which peaks the measure of the complex matrices on unitary matrices. In the limit $\lambda \rightarrow 0$, one recovers Wilson's theory. It is natural therefore to associate small λ with small a . For small λ one can derive a series of corrections to the Wilson action $\text{Tr}_P[U]$ as an expansion in λ . Define the

complex matrix

$$C(l) = \sqrt{\frac{N}{\lambda}} [M(l) - U(l)] . \quad (4)$$

If $1_P, 2_P, 3_P,$ and 4_P are the four links that form plaquette P , we have

$$Z = \int \prod_l \mathcal{D}U(l) \exp \left(\frac{1}{g_L^2} \left(\sum_P \text{Tr}_P[U] \right) + \frac{1}{g_L^2} \Delta V[U] \right) \quad (5)$$

where

$$\begin{aligned} \exp \left(\frac{1}{g_L^2} \Delta V[U] \right) &= \int \prod_l \mathcal{D}C(l) \exp \left(- \sum_l \text{Tr} \{ C^\dagger(l) C(l) \} \right. \\ &\quad \left. + \frac{\sqrt{\lambda}}{g_L^2 \sqrt{N}} \sum_P \text{Tr} \{ C(1_P) U(2_P) U(3_P) U(4_P) + U(1_P) C(2_P) U(3_P) U(4_P) \right. \\ &\quad \left. + U(1_P) U(2_P) C(3_P) U(4_P) + U(1_P) U(2_P) U(3_P) C(4_P) \right\} + O(\lambda) \end{aligned} \quad (6)$$

and we have dropped an irrelevant normalisation constant. Performing the Gaussian integrals over $C(l)$ one generates an effective action for U -variables consisting of arbitrary Wilson loops:

$$\text{Tr}_P[U] + \Delta V[U] = \sum_P \left[4 \left(\begin{array}{|c|} \hline 3 \\ \hline \square \\ \hline 1 \\ \hline \end{array} \right)^2 + \frac{\lambda}{N g_L^2} \left(4 \left(\begin{array}{|c|} \hline 3 \\ \hline \square \\ \hline 1 \\ \hline \end{array} \right)^2 + 4 \left(\begin{array}{|c|} \hline 3 \\ \hline \square \\ \hline 1 \\ \hline \end{array} \right)^2 + 4 \left(\begin{array}{|c|} \hline 3 \\ \hline \square \\ \hline 1 \\ \hline \end{array} \right)^2 + 4 \left(\begin{array}{|c|} \hline 3 \\ \hline \square \\ \hline 1 \\ \hline \end{array} \right)^2 \right] + O(\lambda^2) . \quad (7)$$

(Only the terms in one plane are shown.) The leading correction is the well known rectangular U -loop which, with the correct coefficient, will cancel $O(a^2)$ errors of the Wilson action. One might imagine that by introducing a sufficiently complicated smearing function one could produce systematically the terms needed to correct for higher lattice spacing errors, *id est* a perfect action which tracks an infrared stable RG trajectory [12]. With the simple Gaussian smearing, the first correction to Wilson's action (7) in fact has the wrong sign for improvement. However we are free to make the effective potential more sophisticated beyond the Gaussian approximation by explicitly adding zero-area Wilson M -loops (which become trivial in the limit $\lambda \rightarrow 0$) to the action (2);

$$\begin{aligned} &\sum_l \text{Tr} \{ M^\dagger(l) M(l) M^\dagger(l) M(l) \} , \quad \sum_l (\text{Tr} \{ M^\dagger(l) M(l) \})^2 \\ &\sum_{\langle l, l' \rangle} \text{Tr} \{ M(l) M(l') M^\dagger(l') M^\dagger(l) \} , \quad \textit{et cetera}; \end{aligned} \quad (8)$$

$\langle l, l' \rangle$ denotes a sum over neighboring links. Note that gauge invariance

$$M(l) \rightarrow V_{l-1, l}^\dagger M(l) V_{l, l+1} , \quad V \in SU(N) \quad (9)$$

provides a strong constraint on the allowed terms we can add at each order in the field M . Contributions to the effective potential of the form

$$\frac{N\nu}{\lambda} \text{Tr} \{ M(l) M(l+a) M^\dagger(l+a) M^\dagger(l) \} , \quad (10)$$

where $\nu > 0$ and $l+a$ is the link consecutive to l (parallel to l and sharing one site), will be necessary in the small lattice spacing limit $\lambda \rightarrow 0$ in order to have any chance of producing the correct sign for the coefficient of the leading rectangular U -plaquette correction: the coefficient in Eqn. (7) now becomes $\lambda(1 - 2\nu)/g_L^2 N$. Such terms have generally been neglected in previous studies of dielectric lattice gauge theory.

We may instead integrate out the U -variables link-by-link using the large- N saddle-point result of Ref. [13]. Thus, for some link l ,

$$\int \mathcal{D}U \exp\left(-\frac{N}{\lambda} \text{Tr}\{(M - U)(M^\dagger - U^\dagger)\}\right) = \exp\left(-N^2 x - N \sum_{i=1}^N (\lambda \Lambda_i - 2\sqrt{\Lambda_i + x}) - \frac{1}{2} \sum_{i,j=1}^N \log(\sqrt{\Lambda_i + x} + \sqrt{\Lambda_j + x}) - N^2 \left(\frac{3}{4} + \frac{1}{\lambda}\right)\right) \quad (11)$$

where Λ_i are the eigenvalues of MM^\dagger/λ^2 and

$$x = 0 \quad \text{if} \quad \frac{1}{N} \sum_{i=1}^N \frac{1}{\sqrt{\Lambda_i}} < 2$$

$$\frac{1}{N} \sum_{i=1}^N \frac{1}{\sqrt{x + \Lambda_i}} = 2 \quad \text{if} \quad \frac{1}{N} \sum_{i=1}^N \frac{1}{\sqrt{\Lambda_i}} > 2 \quad (12)$$

Note that λ and Λ_i are $O(1)$ while the effective action is $O(N^2)$ and $g_L^2 N$ is, as usual, held finite in the large N limit. The asymptotics of the effective M -potential (11) versus $\text{Tr}\{M^\dagger M\}/N$ are easily found: for large eigenvalues Λ_i we are in the $x = 0$ regime and so (11) becomes

$$\exp\left(-\frac{N}{\lambda} \text{Tr}\{M^\dagger M\}\right), \quad \frac{1}{N} \text{Tr}\{M^\dagger M\} \rightarrow \infty; \quad (13)$$

for small Λ_i we are in the $x \neq 0$ regime and may expand in powers of Λ_i

$$x = \frac{1}{4} - \frac{1}{N\lambda^2} \text{Tr}\{M^\dagger M\} + O(M^4/\lambda^4) \quad (14)$$

to obtain

$$\exp\left(\left(\frac{-1}{\lambda} + \frac{1}{\lambda^2}\right) N \text{Tr}\{M^\dagger M\} + O(M^4/\lambda^4)\right), \quad \frac{1}{N} \text{Tr}\{M^\dagger M\} \rightarrow 0. \quad (15)$$

As λ is reduced through 1 the (classical) minimum shifts from $M = 0$ to $\text{Tr}\{M^\dagger M\} > 0$. We should not take too seriously the details of the potential derived from (11) beyond the Gaussian approximation, since the additional terms (8) must then be taken into account.

We see the qualitative picture anticipated for the dielectric formulation emerging. At large enough lattice spacing (large enough λ), the effective U -potential (7), which contains arbitrary Wilson loops with roughly equal weight, would be re-organised by the dielectric variables into a

small-field expansion about $M = 0$. In practice one will have to truncate the small-field expansion and the form of the effective M -potential should be fixed by scaling analysis. It is difficult to do this analytically because, apart from the mass of the M -field, there is no identifiably small coupling at hand; $\lambda > 1$ is not small, so we cannot perform improvement near the fixed point, as is now popular in the ELMC approach [14]. In fact, the ultimate justification for expecting a truncation to work comes from light-cone quantisation, as we argue in the next section. (We will use an effective potential truncated to fourth order in the fields (35).) We anticipate that there should be an optimal ‘window’ for use of such a truncated potential. A heavy M -field, when the minimum at $M = 0$ is steep, presumably implies that one is deep in the dielectric regime, where the lattice spacing must be very large (analogous to the very strong coupling regime of Wilson’s theory); in this case any truncation of higher order terms in $V[M]$ may result in severe finite lattice spacing errors. On the other hand our Hamiltonian analysis will only be valid for quantisation about the $M = 0$ classical solution, so the mass squared of the M -field must be positive. This suggests we should take it to be positive and small. Our results will bear this out.

Finally we note that one would arrive at basically the same conclusions for an Abelian theory. However it is well-known that there is a phase transition between strong and weak coupling in this case [8, 15]. The dielectric formulation in the regime where M has positive mass squared would correspond to strong coupling, and is thus not useful for studying weakly coupled QED.

3 Light-cone Hamiltonian formulation

3.1 Transverse lattice

A Hamiltonian limit of the dielectric lattice theory requires us to take the lattice spacing to zero in at least one direction. We now specialise to $2 + 1$ dimensions, since it is for this case that we will perform explicit calculations. Since we also wish to make use of the fact that two components of the vector potential A_μ are non-dynamical, we take the continuum limit in the x^0 and x^2 directions, leaving the transverse direction x^1 discrete. This means that only dynamical degrees of freedom will be involved in the effective potential $V[M]$, a simplification not shared by the Euclidean lattice or equal-time Hamiltonian quantisation of this problem. We now use different smearing parameters λ and $\tilde{\lambda}$ for the transverse x^1 and longitudinal (x^0, x^2) directions, respectively; likewise we define transverse and longitudinal lattice spacings a and \tilde{a} . For the longitudinal directions we take the limit $\tilde{\lambda}, \tilde{a} \rightarrow 0$ so the measure becomes infinitely peaked on unitary matrices; this ensures that

$$\lim_{\tilde{\lambda}, \tilde{a} \rightarrow 0} M(l) = U(l) = 1 + i\tilde{a}A_\alpha + \dots \quad (16)$$

for a link l in the direction $\alpha = 0$ or 2 . Applying Eqn. (16) to $\text{Tr}_P[M]$ one derives a transverse lattice action whose form was first suggested in Ref. [1]

$$A = \int dx^0 dx^2 \sum_{x^1} \left(\text{Tr} \{ D_\alpha M_{x^1} (D^\alpha M_{x^1})^\dagger \} - \frac{a}{4g^2} \text{Tr} \{ F_{\alpha\beta} F^{\alpha\beta} \} - V_{x^1}[M] \right) \quad (17)$$

where

$$D_\alpha M_{x^1} = (\partial_\alpha + iA_\alpha(x^1)) M_{x^1} - iM_{x^1} A_\alpha(x^1 + a) \quad (18)$$

We have introduced the dimensionful continuum gauge coupling³ $g^2 = ag_L^2/\tilde{a}^2$ in $2+1$ dimensions and rescaled $M \rightarrow Mg_L$. M_{x^1} lies on the link between x^1 and $x^1 + a$ while $A_\alpha(x^1)$ is associated with the site x^1 . $V_{x^1}[M]$ is a purely transverse gauge invariant effective potential, which is assumed analytic about its minimum at $M = 0$. For $2+1$ dimensions this means it contains only (products of) zero-area Wilson loops such as those displayed in (8) with one point pinned at x^1 .

A feature of light-cone formalism, which is not present in the equal-time approach, is that for free fields of mass squared $\mu^2 > 0$ the momentum $k^+ = (k^0 + k^2)/\sqrt{2}$ is positive definite for finite energy since

$$k^- = \frac{\mu^2 + (k^1)^2}{2k^+} \quad (19)$$

This, together with momentum conservation, implies that even the quantum vacuum is free of particles and that a large number of particles necessarily carry a large light-cone energy. It is for this reason that one believes a calculation of the low mass spectrum using the light-cone Hamiltonian is feasible when effects due to large numbers of particles have been truncated. Higher powers of the field M in the effective potential couple precisely to those components of the wavefunction with a large number of M -quanta. Of course, in the LCTL construction, the M -quanta are also link variables, so energy considerations are intimately tied in with questions of spacetime symmetry restoration. Note that the above arguments break down if applied to the gluon fields A_1 directly since they are massless and can be produced copiously for $k^1 = 0$. On the other hand, if one gives the gluons A_1 a fake mass this breaks gauge invariance leading to copious production of non-local terms in the effective potential.

3.2 Gauge symmetry

Having formulated a transverse lattice action (17) we now introduce light-cone co-ordinates $x^\pm = (x^0 \pm x^2)/\sqrt{2}$ and quantise by treating x^+ as canonical time, following Ref. [1]. The theory has a conserved current

$$J^+(\mathbf{x}) = i \left[M_{x^1} (D_- M_{x^1})^\dagger - (D_- M_{x^1}) M_{x^1}^\dagger + M_{x^1-a}^\dagger D_- M_{x^1-a} - (D_- M_{x^1-a})^\dagger M_{x^1-a} \right] \quad (20)$$

³ Note that this definition of g^2 differs from the standard one by a factor of 2.

at each transverse lattice site x^1 which plays a special role. If we pick the light-cone gauge⁴ $A_- = 0$ the non-propagating field A_+ satisfies a simple constraint equation at each transverse site

$$(\partial_-)^2 A_+(x^1) = \frac{g^2}{a} J_{x^1}^+ . \quad (21)$$

Solving this constraint leaves an action in terms of the dynamical fields M_{x^1}

$$A = \int dx^+ dx^- \sum_{x^1} \text{Tr} \left\{ \partial_\alpha M_{x^1} \partial^\alpha M_{x^1}^\dagger + \frac{g^2}{2a} J_{x^1}^+ \frac{1}{(\partial_-)^2} J_{x^1}^+ \right\} - V_{x^1}[M] , \quad (22)$$

the pole in the A_+ propagator given by $1/(\partial_-)^2$ is regulated by a principle value type prescription [1, 18]. It is straightforward to derive light-cone momentum and energy

$$P^+ = 2 \int dx^- \sum_{x^1} \text{Tr} \left\{ \partial_- M_{x^1} \partial_- M_{x^1}^\dagger \right\} \quad (23)$$

$$P^- = \int dx^- \sum_{x^1} V_{x^1}[M] - \frac{g^2}{2a} \text{Tr} \left\{ J_{x^1}^+ \frac{1}{\partial_-^2} J_{x^1}^+ \right\} \quad (24)$$

There remains residual gauge symmetry under x^- -independent transformations at each site x^1

$$M_{x^1} \rightarrow V_{x^1+a}^\dagger M_{x^1} V_{x^1} , \quad V \in SU(N) \quad (25)$$

Evidently the light-cone energy (24) will not be finite unless the associated charge vanishes at each site x^1

$$\int_{-\infty}^{+\infty} dx^- J_{x^1}^+ = 0 \quad (26)$$

This requirement also follows from the zero momentum limit of the constraint equation (21) and will force one to consider only singlet states under the transformations (25). This condition is analogous to the colour neutrality imposed by Kogut and Susskind [16] as a consequence of Gauss' law, but here it follows from dynamical considerations alone.

3.3 The Hilbert space

Expanding in harmonic modes at $x^+ = 0$ about $M = 0$, it is convenient to work in longitudinal momentum space and transverse position space

$$M_{x^1}(x^-) = \frac{1}{\sqrt{4\pi}} \int_0^\infty \frac{dk}{\sqrt{k}} \left(a_{-1}(k, x^1) e^{-ikx^-} + (a_{+1}(k, x^1))^\dagger e^{ikx^-} \right) \quad (27)$$

where the modes satisfy equal- x^+ commutators

$$\left[a_{\lambda, ij}(k, x^1), (a_{\rho, kl}(\tilde{k}, \tilde{x}^1))^\dagger \right] = \delta_{ik} \delta_{jl} \delta_{\lambda\rho} \delta_{x^1 \tilde{x}^1} \delta(k - \tilde{k}) \quad (28)$$

$$\left[a_{\lambda, ij}(k, x^1), a_{\rho, kl}(\tilde{k}, \tilde{x}^1) \right] = 0 \quad (29)$$

⁴We set the associated zero mode $\int dx^- A_-$ to zero as a dynamical approximation.

with colour indices $i, j \in \{1, \dots, N\}$, orientation indices $\lambda, \rho \in \{-1, +1\}$; $(a_{\lambda, ij})^\dagger = (a_\lambda^\dagger)_{ji}$ and for clarity we omit the $+$ superscript on k . The Fock space operator $a_{\pm 1}^\dagger(k, x^1)$ creates a mode on the link between sites x^1 and $x^1 + a$ with longitudinal momentum k and orientation ± 1 . In the Fock space, only combinations singlet under (25) are annihilated by the charge (26). This gives a Hilbert space at fixed x^+ formed from all possible closed Wilson loops of link modes a_\pm on the transverse lattice. Thus, a typical p -link loop will be something like

$$\text{Tr} \left\{ a_{+1}^\dagger(k_1, x^1) a_{-1}^\dagger(k_2, x^1) a_{-1}^\dagger(k_3, x^1 - a) \cdots a_{+1}^\dagger(k_p, x^1 - a) \right\} |0\rangle \quad (30)$$

The number of $+1$'s equals the number of -1 's for a closed loop on the transverse lattice, while the longitudinal momenta k_m are unconstrained except for $\sum_{m=1}^p k_m = P^+$ and $k_m \geq 0$. By an abuse of language, we will often refer to p as the number of particles — the link variables are reminiscent of constituents — even though the relevant field variables are non-locally defined. At large N we need only study the dynamics of single connected Wilson loops in the Hilbert space — there are no terms with more than one trace — since the loop-loop coupling constant is of order $1/N$. These loops may be thought of as ‘bare’ glueballs, and the problem is to find the linear combinations that are on mass shell. Neglecting $k_m = 0$, which is consistent with expanding about the $M = 0$ solution of the dielectric regime, the Fock vacuum is an eigenstate of the full light-cone Hamiltonian $P^- |0\rangle = P^+ |0\rangle = 0$.

3.4 Eguchi-Kawai reduction

A further simplification occurring at large N is Eguchi-Kawai reduction [10]. This means that in the Lorentz frame $P^1 = 0$ the theory is isomorphic to one compactified on a one-link transverse lattice with periodic boundary conditions, where P^α acts on a basis of zero winding number Wilson loops [17], *id est* we can simply drop the argument x^1 or l from M in all of the previous expressions. Effectively one is now dealing with a $1 + 1$ -dimensional gauge theory coupled to a complex scalar field in the adjoint representation (with self-interactions). Mathematically isomorphic “collinear QCD models” have recently been studied [20], the equivalence following after identifying winding number (orientation) here with helicity there.

The Eguchi-Kawai reduced states corresponding to $P^1 = 0$ and fixed P^+ can now be written as colour singlet Fock basis states on one link. A general state expanded in terms the orthonormal basis is then (summation on repeated indices implied)

$$|\Psi\rangle = \sum_{\substack{p=|n|, |n|+2, \dots \\ p>0}} \int_0^{P^+} \frac{dk_1 \cdots dk_p}{N^{p/2}} \delta(P^+ - \sum_{m=1}^p k_m) f^{\lambda\rho \dots \sigma}(k_1, \dots, k_p)$$

$$\cdot \text{Tr} \left\{ a_\lambda^\dagger(k_1) a_\rho^\dagger(k_2) \cdots a_\sigma^\dagger(k_p) \right\} |0\rangle \quad (31)$$

where we set the winding number $n = \lambda + \rho + \cdots + \sigma$ equal to zero. When the wavefunctions f are chosen appropriately, the states $|\Psi\rangle$ will describe an infinite discrete set of stable physical glueballs satisfying the mass shell condition.

Using the mode expansion of the operators P^α in Fock space, one may explicitly verify that the isomorphism under reduction holds. Some details of this calculation and its validity are given in Appendix A. The reduction rests on expanding about the $M = 0$ classical solution. We have already argued that, at sufficiently small lattice spacing, the classical minimum is no longer at $M = 0$, and our quantisation is no longer valid. Note that this is not a statement about equivalence under reduction breaking down, but about our entire method, whether applied to the reduced or unreduced theory. Wilson's lattice gauge theory in the Lagrangian formulation is valid for any correlation length, but Eguchi-Kawai reduction breaks down at small lattice spacing [19] and various quenching and twisting prescriptions have been given in order to approach the critical surface in coupling constant space with a reduced theory. The dielectric formulation with expansion about $M = 0$ does not need quenching/twisting, but we pay for this by having to work with an effective theory at rather large lattice spacing on the scaling trajectory.

3.5 Symmetries

The theory possesses several discrete symmetries. Charge conjugation induces the symmetry

$$\mathcal{C} : a_{+1,ij}^\dagger \leftrightarrow a_{-1,ji}^\dagger . \quad (32)$$

There are two orthogonal reflection symmetries \mathcal{P}_1 and \mathcal{P}_2 either of which may be used as ‘parity’. If $\mathcal{P}_1 : x^1 \rightarrow -x^1$, we have

$$\mathcal{P}_1 : a_{+1,ij}^\dagger \leftrightarrow a_{-1,ij}^\dagger . \quad (33)$$

$\mathcal{P}_2 : x^2 \rightarrow -x^2$, is more subtle in light-cone quantisation since it does not preserve the quantisation surface. Its explicit operation is known for sure only for a set of p free particles [22], which we call

$$\mathcal{P}_{2f} : \frac{k_m}{P^+} \rightarrow \left(k_m \sum_{m'=1}^p \frac{1}{k_{m'}} \right)^{-1} . \quad (34)$$

The latter \mathcal{P}_{2f} is nevertheless useful since it is often an approximate quantum number and its expectation value can be used to estimate \mathcal{P}_2 [20, 21]. Given \mathcal{P}_2 and \mathcal{P}_1 we can determine whether spin \mathcal{J} is even or odd using the relation $(-1)^\mathcal{J} = \mathcal{P}_1 \mathcal{P}_2$. If rotational symmetry has been restored in the theory, states of spin $\mathcal{J} \neq 0$ should form degenerate \mathcal{P}_1 doublets $|+\mathcal{J}\rangle \pm |-\mathcal{J}\rangle$ [9]. We use “spectroscopic notation” $|\mathcal{J}|^{\mathcal{P}_1 \mathcal{C}}$ to classify states.

3.6 The effective potential

The basis written in (31) is already diagonal in P^+ , and P^+ commutes with P^- . It remains to find the coefficient functions f , cyclically symmetric in their arguments, which diagonalise the Hamiltonian P^- and hence the Lorentz invariant (mass)² operator $2P^+P^-$ with eigenvalue M^2 . Before proceeding we must choose the explicit form of the transverse effective potential. In this work, we will include in $V[M]$ all Wilson loops and products of Wilson loops up to fourth order in link fields M . After Eguchi-Kawai reduction this limits one to the following form

$$\begin{aligned}
V[M] = & \mu^2 \text{Tr} \{MM^\dagger\} + \frac{\lambda_1}{aN} \text{Tr} \{MM^\dagger MM^\dagger\} \\
& + \frac{\lambda_2}{aN} \text{Tr} \{MM^\dagger M^\dagger M\} + \frac{\lambda_3}{aN^2} \text{Tr} \{M^\dagger M\} \text{Tr} \{M^\dagger M\}
\end{aligned} \tag{35}$$

Note that the last term above, which might appear suppressed at large N , is in fact non-zero only for 2-link Fock states ($p = 2$ in Eqn. (31)). It is a term which ‘pinches’ the worldsheet swept out in light-cone time x^+ by the glueball flux ring given by the superposition of Wilson loops (31). Near a critical surface in coupling constant space it is naively irrelevant, but at finite lattice spacing it turns out to be quite significant. In principle one should repeat calculations with higher orders of the field allowed in the action, to determine the magnitude of any changes. We will not be able to do this with our modest computing resources — there are many more allowed terms at 6th order — but will look at other quantities, such as expectation values of higher order Wilson loops, in order to assess effects of this truncation. (One can also of course compare with results obtained using only the quadratic term in (35)). Our goal is to find out if there is a trajectory in the parameter space of (35) along which physical quantities scale *and* agree with the ELMC simulations [9] with reasonable χ^2 .

The renormalisation of the quantum theory at fixed lattice spacing follows that of a 2D gauge theory with adjoint matter [20], involving only logarithmically divergent self-energy subtractions on the propagator and a principle value prescription for the light-cone Coulomb singularity. Explicitly one finds at large N

$$P^+ = \int_0^\infty dk k \text{Tr} \{a_\lambda^\dagger(k) a_\lambda(k)\} \tag{36}$$

$$\begin{aligned}
P^- = & \frac{\mu^2}{2} \int_0^\infty \frac{dk}{k} \text{Tr} \{a_\lambda^\dagger(k) a_\lambda(k)\} \\
& + \text{P} \int_0^\infty \frac{dk_1 dk_2 dk_3 dk_4}{8\pi a \sqrt{k_1 k_2 k_3 k_4}} [\delta(k_1 + k_2 - k_3 - k_4) \mathcal{H}_{2 \rightarrow 2} \\
& + \delta(k_1 + k_2 + k_3 - k_4) (\mathcal{H}_{1 \rightarrow 3} + \mathcal{H}_{3 \rightarrow 1})]
\end{aligned} \tag{37}$$

where

$$\begin{aligned}
\mathcal{H}_{2 \rightarrow 2} &= \left(\frac{\lambda_1}{N} - \frac{g^2 (k_2 - k_1) (k_4 - k_3)}{(k_1 + k_2)^2} \right) \text{Tr} \left\{ a_\lambda^\dagger(k_1) a_{-\lambda}^\dagger(k_2) a_\rho(k_3) a_{-\rho}(k_4) \right\} \\
&+ \left(\frac{\lambda_1}{N} - \frac{g^2 (k_2 + k_3) (k_1 + k_4)}{(k_2 - k_3)^2} \right) \text{Tr} \left\{ a_\lambda^\dagger(k_1) a_\rho^\dagger(k_2) a_\rho(k_3) a_\lambda(k_4) \right\} \\
&+ \frac{(\lambda_2 - \lambda_1)}{N} \text{Tr} \left\{ a_\lambda^\dagger(k_1) a_\rho^\dagger(k_2) a_\lambda(k_3) a_\rho(k_4) \right\} \\
&+ \frac{\lambda_3}{2N^2} \text{Tr} \left\{ a_\lambda^\dagger(k_1) a_{-\lambda}^\dagger(k_2) \right\} \text{Tr} \left\{ a_\rho(k_3) a_{-\rho}(k_4) \right\} \tag{38}
\end{aligned}$$

$$\begin{aligned}
\mathcal{H}_{1 \rightarrow 3} &= \left(\frac{\lambda_1}{N} - \frac{g^2 (k_2 - k_1) (k_4 + k_3)}{(k_1 + k_2)^2} \right) \text{Tr} \left\{ a_\lambda^\dagger(k_1) a_{-\lambda}^\dagger(k_2) a_\rho^\dagger(k_3) a_\rho(k_4) \right\} \\
&+ \left(\frac{\lambda_1}{N} - \frac{g^2 (k_2 - k_3) (k_1 + k_4)}{(k_2 + k_3)^2} \right) \text{Tr} \left\{ a_\lambda^\dagger(k_1) a_\rho^\dagger(k_2) a_{-\rho}^\dagger(k_3) a_\lambda(k_4) \right\} \\
&+ \frac{(\lambda_2 - \lambda_1)}{N} \text{Tr} \left\{ a_\lambda^\dagger(k_1) a_\rho^\dagger(k_2) a_{-\lambda}^\dagger(k_3) a_\rho(k_4) \right\} \tag{39}
\end{aligned}$$

$$\mathcal{H}_{3 \rightarrow 1} = \mathcal{H}_{1 \rightarrow 3}^\dagger. \tag{40}$$

In the $N = \infty$ limit we do not distinguish $U(N)$ from $SU(N)$ and the gauge coupling $g^2 N$ is finite. The light-cone Schrödinger equation defined by taking the matrix elements $\langle \text{Fock} | 2P^+ P^- | \Psi \rangle = M^2 \langle \text{Fock} | \Psi \rangle$ allows one to write down an infinite set of successively coupled integral equations for the corresponding Fock components f . We do not bother to list them here since they are rather complicated, but refer the reader to Ref. [20] for equivalent expressions. To diagonalise P^- we will employ a combination of variational ansätze for the f 's and numerical solution through discretisation the momenta k and truncation of the number of particles p .

4 The glueball spectrum

4.1 Analytic wavefunctions

The behavior of the wavefunctions f in Eqn. (31) when any one of the arguments vanishes [1] is

$$\lim_{k_i \rightarrow 0} f_{\lambda \rho \dots \sigma}(k_1, k_2, \dots, k_p) \propto k_i^\beta \quad \text{where} \quad 2\beta \tan(\pi\beta) = \frac{a\mu^2}{g^2 N} \tag{41}$$

and $0 < \beta < 1/2$. Specifying also the number of nodes of f as a function of momenta, one can make a sensible ansatz. For λ_1 and λ_2 small there is very little mixing between Fock states of different number of link modes p [20]. In this case a mass eigenstate $|\Psi\rangle$ has predominantly a fixed p , the mass increasing with p . For a given p , the energy also tends to increase with the number of nodes in the wavefunction f due to the $J(\partial_-)^{-2} J$ term in (24), which is in fact a positive contribution.

Thus one naively expects the lowest two eigenstates to be approximately

$$\int_0^{P^+} dk f_{+1,-1}(k, P^+ - k) \text{Tr} \left\{ a_{+1}^\dagger(k) a_{-1}^\dagger(P^+ - k) \right\} |0\rangle \quad (42)$$

with the lowest state having a symmetric wavefunction $f_{+1,-1}(k, P^+ - k)$, corresponding to 0^{++} , and first excited state having $f_{+1,-1}$ antisymmetric with one node, corresponding to 0^{--} . The next highest states are either a 4-link state with positive symmetric wavefunctions $f_{+1,+1,-1,-1}$ and $f_{+1,-1,+1,-1}$ or a symmetric 2-link state with $f_{+1,-1}$ having two nodes. In the glueball spectrum we identify the latter states as 0_*^{++} and 2^{++} , respectively, although actual eigenstates are a mixture of these. The above naive considerations correctly predict the ordering of light glueballs in the spectrum, but differ in the details of the wavefunctions we find numerically later.

In light of the endpoint analysis (41), it is useful to consider wavefunctions f in Eqn. (31) with the simplified longitudinal form k_i^β and arbitrary transverse structure: a ‘‘transverse only’’ model. Thus we construct a basis of unit norm states of the form:

$$|\sigma_1, \dots, \sigma_p\rangle = C_{\sigma_1, \dots, \sigma_p} \sqrt{\frac{\Gamma(2\beta p + p)}{N^p \Gamma(2\beta + 1)^p}} \int dk_1 \cdots dk_p \text{Tr} \left\{ a_{\sigma_1}^\dagger(k_1) \cdots a_{\sigma_p}^\dagger(k_p) \right\} |0\rangle \cdot \delta \left(p^+ - \sum_i k_i \right) (k_1 \cdots k_p)^\beta \quad (43)$$

where $\sigma_i \in \{-1, +1\}$ and we set the winding number $n = \sum_i \sigma_i$ to zero. One can characterise these states with the ‘‘folding parameter’’ γ :

$$p\gamma = \text{The number of } i \text{ such that } \sigma_i = \sigma_{i+1}. \quad (44)$$

Thus,

$$p(1 - \gamma) = \text{The number of } i \text{ such that } \sigma_i \neq \sigma_{i+1}. \quad (45)$$

(Here, one should think of a 1-dimensional polymer model.) Roughly speaking, the transverse size of a typical state is $a(p/2)^\gamma$. Using γ , we can write down an exact expression for the expectation value of the Lorentz invariant $(\text{mass})^2$ operator:

$$\begin{aligned} & \langle \sigma_1, \dots, \sigma_p | P_\mu P^\mu | \sigma_1, \dots, \sigma_p \rangle \\ &= p(p(1 + 2\beta) - 1) \cdot \\ & \quad \left(\frac{\mu^2}{2\beta} + \frac{\Gamma(\beta + 1/2)^4 \Gamma(1 + 4\beta)}{4\pi a \Gamma(1 + 2\beta)^4} [g^2 N(1 + 4\beta) + 2(1 - \gamma)\lambda_1 + \gamma\lambda_2] \right), \quad p > 2 \quad (46) \\ &= \frac{p^2 \pi}{4a} (g^2 N + 2(1 - \gamma)\lambda_1 + \gamma\lambda_2) \\ & \quad + \frac{\beta \pi p^2}{2a} (g^2 N(5 - 4 \ln 2) - (2\lambda_1(1 - \gamma) + \lambda_2 \gamma)(4 \ln 2 - 1)) \\ & \quad + O(p) + O(\beta^2). \quad (47) \end{aligned}$$

For the two particle state $|+1, -1\rangle$ the expectation value of the invariant $(\text{mass})^2$ operator is,

$$\begin{aligned} \langle +1, -1 | P_\mu P^\mu | +1, -1 \rangle &= \frac{\pi}{2a} (g^2 N + 2\lambda_1 + \lambda_2 + \lambda_3) \\ &+ \frac{2\beta\pi}{a} (g^2 N (3 - 2 \ln 2) - (2\lambda_1 + \lambda_2 + \lambda_3) (2 \ln 2 - 1)) \\ &+ O(\beta^2) . \end{aligned} \tag{48}$$

If one demands a positive-definite spectrum, these expressions place variational bounds on the allowed region in parameter space. First we must have positive μ^2 else our quantisation procedure is no longer valid and the spectrum becomes unbounded from below. For the $p = 2$ case the expectation value of the invariant $(\text{mass})^2$ becomes tachyonic when

$$2\lambda_1 + \lambda_2 + \lambda_3 \leq -g^2 N (1 + 8\beta) + O(\beta^2) , \tag{49}$$

while from (46) we see that many particle states become tachyonic at

$$2(1 - \gamma)\lambda_1 + \gamma\lambda_2 \leq -g^2 N (1 + 8\beta) + O(\beta^2) . \tag{50}$$

4.2 Numerical results

In our numerical solutions we restrict the number of link fields p in our basis states (31) and discretise momenta by demanding antiperiodicity of the fields in $x^- \rightarrow x^- + L$. This is a high light-cone energy cut-off since, unlike in the transverse direction, light-cone momentum goes like the inverse of energy. (we use the method of [20] to handle the IR divergence). For fixed integer valued cut-off $K = LP^+/(2\pi)$ momenta are labeled by odd half integers $\kappa_m = Kk_m/P^+$, $K = \sum_m \kappa_m$. On the computer, we generate a basis of states and calculate matrix elements of the Hamiltonian using the hybrid wavefunction/DLCQ matrix elements discussed in Appendix C. The nonzero matrix elements are then stored in a file (the matrix is, in fact, quite sparse). To diagonalise the Hamiltonian P^- , we employ a standard Lanczos algorithm.

In order to fix the coupling constants in the effective potential, we perform a least χ^2 fit to Teper's ELMC large N extrapolated spectrum.⁵ As we shall later show, the mass in units of the coupling $m^2 = \mu^2 a/(g^2 N)$ is a measure of the lattice spacing while the other terms in our effective potential λ_1 , λ_2 , and λ_3 must be found from the fitting procedure. We will also determine $g^2 N/a$ based on a fit, which we check self-consistently with measurements of the string tension.

In order to minimise errors associated with our truncation in p and K , we take the spectra for

$$(K, p \text{ truncation}) \in \{(10, 4), (10, 6), (10, 8), (11, 6), (12, 6), (13, 6), (14, 6)\} \tag{51}$$

⁵For the ELMC data, we assumed rotational symmetry and averaged over parity doubles.

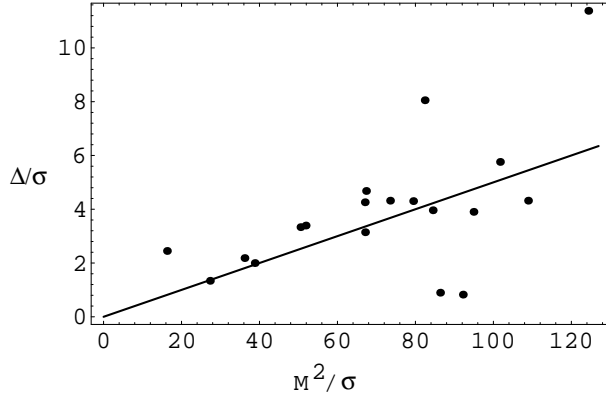


Figure 1: Difference between the unextrapolated and extrapolated eigenvalues $\Delta = \left| M_{K=14, p \leq 6}^2 - M_{\text{extrapolated}}^2 \right|$ vs M^2 for the spectrum in Fig. 3. Also shown is the function $0.05M^2$ which is the assumed size for our error bars.

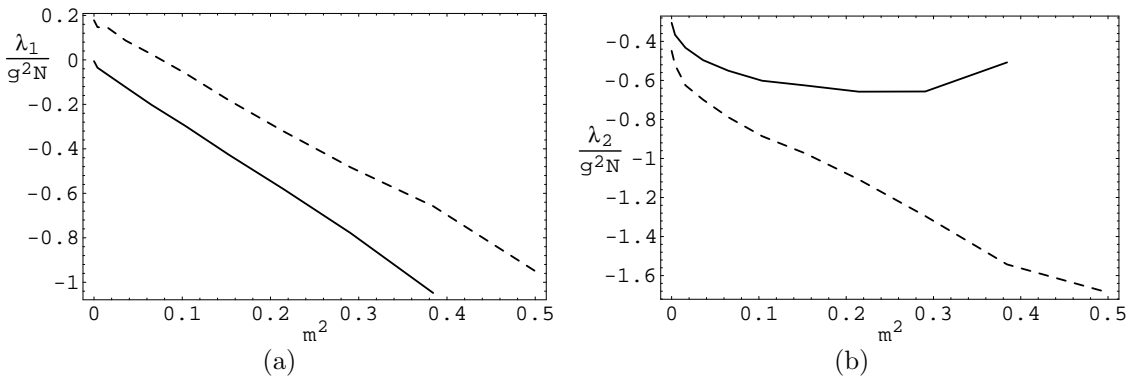


Figure 2: Scaling trajectory in parameter space. We plot (a) $\lambda_1/(g^2N)$ and (b) $\lambda_2/(g^2N)$ vs mass m^2 . The solid line is the data in Table 1; the dashed line is from a second trajectory discussed in Section 4.3.

and extrapolate to the continuum, $K, p \rightarrow \infty$, using a least squares fit to the function

$$c_0 + \frac{c_1}{K} + c_2 e^{cP} \quad (52)$$

where c is given by our estimate in Appendix B and the $1/K$ term is consistent with the leading finite K error as discussed in Appendix C. Since we cannot measure $|\mathcal{J}|$ directly, we only classified states according to \mathcal{P}_1 and \mathcal{C} during the fitting process. In practice we found that the fitting function (52) worked quite well for all but the highest 3 or 4 states where the exponential convergence in p -truncation was not yet evident.⁶ We estimate our one-sigma errors from finite K and p -truncation to be roughly $0.05M^2$; see Fig. 1.

As we fit the various couplings as a function of m^2 , we find a narrow strip in parameter space

⁶However, looking at the $K = 10, p \leq 8$ sector, even these highest states had less than 15% 8-particle content.

$m^2 = \frac{\mu^2 a}{g^2 N}$	$\frac{\lambda_1}{g^2 N}$	$\frac{\lambda_2}{g^2 N}$	$\frac{g^2 N}{a\sigma}$	χ^2	c
0.	-0.00565	-0.305	4.38	30.	-1.43
0.00394	-0.035	-0.366	4.11	25.9	-1.29
0.0158	-0.0677	-0.433	3.84	25.3	-1.2
0.036	-0.123	-0.496	3.65	23.1	-1.1
0.065	-0.202	-0.55	3.47	23.5	-1.01
0.104	-0.297	-0.602	3.28	23.6	-0.94
0.153	-0.427	-0.626	3.1	24.9	-0.884
0.214	-0.58	-0.658	2.97	25.7	-0.832
0.291	-0.778	-0.657	2.84	28.6	-0.792
0.384	-1.05	-0.508	2.67	35.2	-0.802
0.5	—	—	—	—	—

Table 1: Scaling trajectory for the extrapolated spectrum. Here we tabulate couplings vs m^2 for a best χ^2 fit to the ELMC spectrum. We find that $\lambda_3/(g^2 N)$ is always quite large (> 100). We could not find a satisfactory minimum for the $m^2 = 0.5$ datum.

where we obtain good agreement with the ELMC spectrum; see Table 1 and Fig. 2. As we shall see, moving along this strip corresponds to changing the lattice spacing a . The strip, where χ^2 has a local minimum, disappears when m^2 is sufficiently large, indicating that for large enough lattice spacing our truncation of the effective potential is no longer a good approximation.

In Fig. 3, we have plotted a typical spectrum along the scaling trajectory together with the ELMC results. For graphing purposes, we assigned $|\mathcal{J}|$ to our spectrum based on a best fit to Teper's results. As a partial check of this assignment, we calculated the expectation value of \mathcal{P}_{2f} , Eqn. (34), for our spectrum ($K = 10$, $p \leq 6$ truncation). The subsequent determination of $(-1)^{\mathcal{J}}$ agreed with the spectrum fit for most of the low-lying glueballs. However, there was disagreement in the assignment of $(-1)^{\mathcal{J}}$ between the lowest 0^{-+} , first excited 2^{-+} , and lowest 1^{-+} states in Fig. 3. However, since these three levels are almost degenerate, this discrepancy is not important. Of more importance is the $|\mathcal{J}|^{+-}$ sector where our measurements were ambiguous (with $\langle \Psi | \mathcal{P}_{2f} | \Psi \rangle \approx 0$) except for the lowest 2^{+-} state where we obtained the opposite of the desired result for $(-1)^{\mathcal{J}}$.

Although the overall fit with the conventional lattice results is quite good, we see two deficiencies of our spectrum that cannot be attributed to K or p -truncation errors. First, we see that the lowest 0^{--} state is too low in energy. Second, we see that the lowest parity doublet $2^{\pm+}$ is not quite degenerate. We believe that these discrepancies must be due to our truncation of the effective potential. Finally, we have made no prediction for the lowest 1^{++} state since it lies too high in the $|\mathcal{J}|^{++}$ spectrum; there may be a additional 0^{++} state of lower energy which prevents us from labeling the 1^{++} unambiguously.

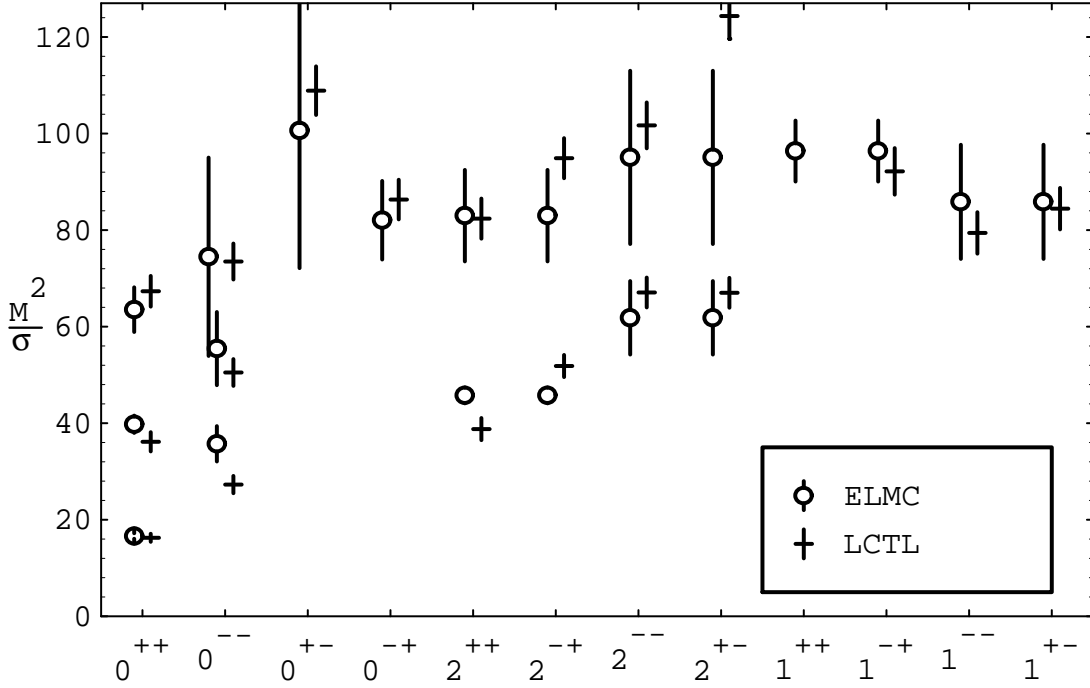


Figure 3: A fit of our LCTL extrapolated results against Teper's ELMC large N extrapolated spectrum [9]. The M^2 eigenvalues are shown in units of (Teper's) string tension for various $|\mathcal{J}|^{P_1 C}$. The parameters are from the $m^2 = 0.065$ row of Table 1. One finds similar spectra along the entire scaling trajectory in coupling constant space.

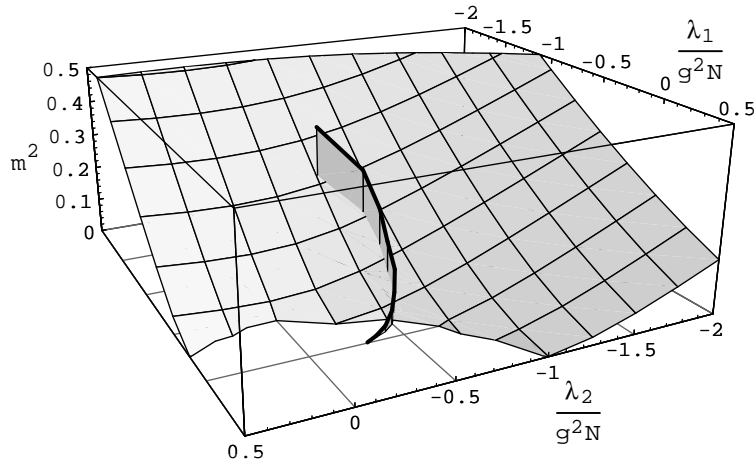


Figure 4: Mass $m^2 = \mu^2 a / (g^2 N)$ such that the lowest M^2 eigenvalue is zero vs $\lambda_1 / (g^2 N)$ and $\lambda_2 / (g^2 N)$ for $p \leq 6$, $K = 14$, $\lambda_3 = 100 g^2 N$. Below this surface the spectrum is tachyonic and below $m^2 = 0$ our quantisation breaks down. The dark line is the scaling trajectory.







$ \mathcal{J} ^{\mathcal{P}_1\mathcal{C}}$	$\frac{M^2}{\sigma}$						
0^{++}	16.3	0.036	0.472	0.372	0.019	0.084	0.017
0^{++}	36.2	0.046	0.359	0.528	0.019	0.024	0.023
0^{++}	67.3	0.051	0.405	0.332	0.026	0.145	0.04
0^{--}	27.3	0.909	0.075	0.011	0.002	0.002	0
0^{--}	50.5	0.06	0.681	0.153	0.037	0.065	0.003
0^{--}	73.5	0.02	0.16	0.741	0.014	0.048	0.018
0^{+-}	109.	0	0.142	0.026	0.026	0.801	0.005
0^{-+}	86.3	0	0.244	0.671	0.01	0.059	0.016
2^{++}	38.8	0.86	0.09	0.033	0.006	0.011	0
2^{++}	82.4	0.022	0.113	0.096	0.078	0.512	0.179
2^{-+}	51.8	0	0.885	0.014	0.027	0.074	0
2^{-+}	94.9	0	0.16	0.036	0.011	0.793	0.001
2^{--}	67.1	0.859	0.082	0.05	0.003	0.005	0.001
2^{--}	102.	0.054	0.609	0.132	0.061	0.136	0.007
2^{+-}	67.	0	0.909	0.003	0.037	0.051	0
2^{+-}	124.	0	0.701	0.126	0.027	0.142	0.004
1^{-+}	92.2	0	0.549	0.156	0.022	0.269	0.003
1^{--}	79.4	0.047	0.398	0.447	0.013	0.081	0.014
1^{+-}	84.4	0	0.895	0.007	0.034	0.063	0

Table 2: The transverse structure of the spectrum for $K = 14$, $p \leq 6$. The first column is our assignment of $|\mathcal{J}|^{\mathcal{P}_1\mathcal{C}}$, the second column is the extrapolated $(\text{mass})^2$ from Fig. 3, and the remaining columns show the probability for a state to have a given transverse structure. The coupling constants are from the $m^2 = 0.065$ row of Table 1.

The numerical bound for absence of tachyons is shown in Fig. 4 as a zero-mass surface. The surface agrees rather well with the analytic bound provided by the “transverse only” model (50) with γ taken over the full range $0 < \gamma < 1$. As the transverse lattice spacing vanishes the mass gap should vanish in lattice units. The fixed point for this, which we believe lies somewhere at negative m^2 , should lie on the zero-mass surface, but is inaccessible to us in the dielectric regime $m^2 > 0$. Nevertheless the scaling trajectory should gradually approach the zero-mass surface if it is to eventually encounter the fixed point. We see this happening already in Fig. 4.

Looking at the transverse structure in Table 2, one can see several important properties of the spectrum. First we notice that the lowest 0^{++} state has very little two particle content. This is the main effect of the $(\text{Tr}\{M^\dagger M\})^2$ interaction when the associated coupling constant λ_3 is large. It

essentially removes the two particle sector from the wavefunction of this state. Second, we notice that there is a relatively large mixing between the various sectors, including mixing of sectors of different particle number at the 10-20% level. This is large enough to restore some rotational invariance but not so large that it contradicts our truncation of the effective potential. If we look at parity doublets, we see that each wavefunction is quite dissimilar from its partner, including very different particle content. This is what one would expect since full parity is dynamically complicated in light-cone coordinates. Finally, one would expect from Regge trajectories that the lowest 2^{++} state would have a large two particle content while the first excited 0^{++} state should not. This helps us label the correct $|\mathcal{J}|$ for these two nearly degenerate states. In fact, large mixing between these states may explain why we do so poorly with the lowest $2^{\mathcal{P}_1+}$ parity doublet.

4.3 Is our spectrum accidental?

Since the scaling trajectory in Table 1 is a *local* minimum of χ^2 in coupling constant space, one might worry that our agreement with the ELMC data is accidental. Since we are not always able to assign $|\mathcal{J}|$ to our states, it is possible that another local minimum in parameter space represents the ‘correct’ scaling trajectory. With this in mind, we have conducted a thorough search of parameter space and have found two other trajectories.

The first occurs for $\lambda_2 \approx 0.5g^2N$ and $\lambda_1 < 0$. However, the χ^2 of the fits are significantly worse. Moreover, it goes against our theoretical prejudice that the scaling trajectory should be in the vicinity of, and track towards, the zero-mass surface (fig.(4)).

The second occurs quite close to our scaling trajectory. We have included λ_1 and λ_2 for this trajectory as dashed lines in Fig. 2. Indeed, the χ^2 of the fits are as good or better than that of our chosen trajectory. We find that the principle difference between the two trajectories is that the 2^{++} and 0^{++} levels are switched — recall that we are unable to distinguish these levels by exact symmetries alone. Consistent with the Regge trajectory picture, we believe that two particle states should form the lowest Regge trajectory and hence the lowest 2^{++} state should contain mainly two particles. Thus, we have chosen the scaling trajectory where the lowest 2^{++} state has mainly two particle content. Additionally, we find that the ratio $(g^2\sigma)_{\text{LCTL}}/(g^2\sigma)_{\text{ELMC}}$ in Fig. 6 is not as good for this other trajectory (dashed line), nor does it appear to track towards the zero-mass surface.

5 The String Tension.

To measure the string tension in the x^1 direction (before Eguchi-Kawai reduction) consider a lattice with n transverse links and periodic boundary conditions. Constructing a basis of Polyakov loops, “winding modes,” that wind once around this lattice, one may extract from the lowest eigenvalue

M^2 vs n the lattice string tension $a\sigma = \Delta M_n/\Delta n$. Because of Eguchi-Kawai reduction, this is equivalent to using Polyakov loops of winding number n on the single-link periodic lattice (Eqn. (31) with $n \neq 0$).

5.1 Analytic results

The behavior of Eqn. (41) is equally true of winding modes $n \neq 0$. Thus, it is useful to extend the “transverse only” model of Section 4.1 to the case of nonzero winding number n . In particular, consider the $p = n$ particle state $|+1, +1, \dots + 1\rangle$ and the $p = n+2$ particle state $|-1, +1, +1, \dots + 1\rangle$. The correct normalisation of these states is

$$1 = \langle +1, +1, \dots + 1 | +1, +1, \dots + 1 \rangle = p C_{+1,+1,\dots,+1}^2 \quad (53)$$

$$1 = \langle -1, +1, +1, \dots + 1 | -1, +1, +1, \dots + 1 \rangle = C_{-1,+1,+1,\dots,+1}^2. \quad (54)$$

Using these two states as a basis, we obtain a 2×2 mass squared matrix ($n > 1$)

$$\frac{1}{4a} \begin{pmatrix} \pi n(n-1)(g^2N + \lambda_2) & 4n\sqrt{n+1}(\lambda_1 + \lambda_2) \\ 4n\sqrt{n+1}(\lambda_1 + \lambda_2) & \pi(n+1)(n+2)(g^2N + \lambda_2) + 4\pi(n+1)\lambda_1 \end{pmatrix} + O(\beta). \quad (55)$$

The diagonal elements come from Eqn. (46), setting $\gamma = 1$ and $\gamma = (n+1)/(n+2)$, respectively. The off-diagonal matrix element is, more precisely,

$$\begin{aligned} & \langle +1, +1, \dots + 1 | P_\mu P^\mu | -1, +1, +1, \dots + 1 \rangle \\ &= \frac{(\lambda_1 + \lambda_2) \Gamma(4\beta + 1) \Gamma(\beta + \frac{1}{2})^3 \sqrt{n} \Gamma((2\beta + 1)n) \Gamma((2\beta + 1)(n + 2))}{2\pi a \Gamma(3\beta + \frac{3}{2}) \Gamma(2\beta + 1)^2 \Gamma(2\beta(n + 1) + n)}. \end{aligned} \quad (56)$$

An example of the lowest eigenvalue of Eqn. (55) vs n is plotted in Fig. 5. For large n one obtains a linear spectrum $M \approx n\sqrt{(\lambda_2 + g^2N)/a}$ and the vanishing lattice string tension condition $\lambda_2 = -g^2N + O(\beta)$.

5.2 Numerical results

Numerical calculation of the winding modes proceeds in the same manner as our calculation of the spectrum except that we use a basis of $n \neq 0$ states. String theory arguments indicate that oscillations of the winding mode transverse to itself yield a form $M^2 = \sigma^2(na)^2 - \sigma\pi/3$, the constant correction being due to Casimir energy [23]. Fig. 5 shows a typical M^2 vs n plot for winding modes. Consistent with the expectations from string theory, we have fit the winding mode spectrum to a curve of the form

$$\frac{M_n^2}{\sigma} = a^2 \sigma n^2 + \frac{b}{\sigma}, \quad (57)$$

which we expect to be appropriate for QCD at sufficiently large n . As illustrated by Fig. 5, there is a good fit to the quadratic. In the same manner, we determine (57) all along the scaling trajectory with the result is shown in Table 3.

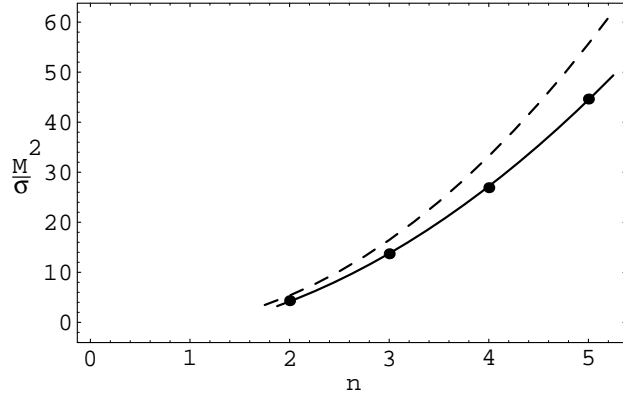


Figure 5: Lowest M^2 eigenvalue vs n for winding modes. Here, $K = 10.5$ or 11 , $p \leq n + 4$, and the couplings are taken from the $m^2 = 0.065$ row of Table 1. Also shown is a numerical fit to $1.92n^2 - 3.5$. The dashed line is from the variational estimate of Eqn. (55). There is a subtlety associated with the $n = 1$ point, which is described in the text.

$m^2 = \frac{\mu^2 a}{g^2 N}$	$a^2 \sigma$	$\frac{b}{\sigma}$
0.	1.48	-2.77
0.00394	1.56	-2.95
0.0158	1.65	-3.08
0.036	1.77	-3.29
0.065	1.92	-3.5
0.104	2.09	-3.68
0.153	2.3	-3.82
0.214	2.55	-4.06
0.291	2.86	-4.28
0.384	3.29	-4.21

Table 3: String tension measurements along the scaling trajectory. The coupling constants are taken from Table 1. Here, the lowest winding mode eigenvalue M_n^2/σ has been fit to $a^2 \sigma n^2 + b/\sigma$ for $n = 2, 3, 4, 5$.

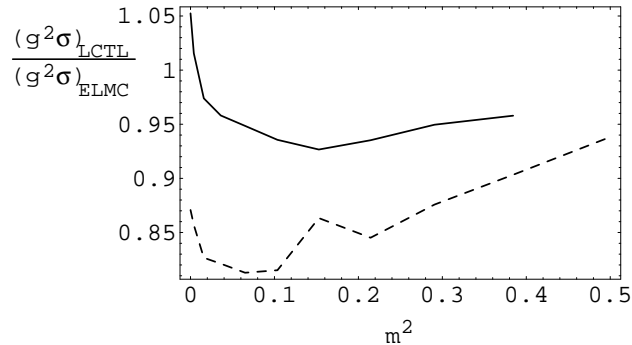


Figure 6: The ratio $(g^2\sigma)_{\text{LCTL}}/(g^2\sigma)_{\text{ELMC}}$. The solid line is for our scaling trajectory while the dashed line is from the second trajectory discussed in Section 4.3.

The constant term b/σ represents the leading finite transverse size correction to the string tension, and is supposed to be universal. The fact that it varies strongly along our ‘scaling trajectory’, shows that for this quantity there are still large finite a errors. Also we have not extrapolated in K or p truncation. There is a subtlety associated with the $n = 1$, one particle matrix element

$$\frac{1}{N} \langle 0 | \text{Tr} \{ a_1(K) \} P_\mu P^\mu \text{Tr} \{ a_1^\dagger(K) \} | 0 \rangle . \quad (58)$$

The most consistent definition is to assume that this matrix element is infinite due to the diagonal part of the $J(\partial_-)^{-2}J$ interaction. In this case, $M_{n=1}^2$ lies somewhat above the extrapolation of the solid line in Fig. 5 down to $n = 1$, since the eigenfunction contains only 3, 5, 7, ...-particle contributions. (If one instead defines (58) to be equal to μ^2 , $M_{n=1}^2$ falls right along the extrapolation of the quadratic fit.) We have not included the $n = 1$ datum in our determination of the string tension.

If we are careful to distinguish between our measurement of g^2N and σ versus g^2N and σ used in the ELMC calculations, we can form the ratio

$$\frac{(g^2\sigma)_{\text{LCTL}}}{(g^2\sigma)_{\text{ELMC}}} = \left(\frac{\sqrt{\sigma}}{g^2N} \right)_{\text{ELMC}} \cdot \frac{(g^2N)_{\text{LCTL}}}{a\sigma_{\text{ELMC}}} \cdot \sqrt{\frac{a^2\sigma_{\text{LCTL}}^2}{\sigma_{\text{ELMC}}}} \quad (59)$$

The first term is 0.1974(12) according to Teper’s large N extrapolated measurement of $\sqrt{\sigma}/(g^2N)$ and the remaining two terms are from Tables 1 and 3, respectively. This ratio measures our error in measuring the string tension plus any discrepancy between g^2N as used by us and that used in the ELMC calculation. From Fig. 6, we see that the two couplings differ by 5%. This implies a rather large discrepancy since we have used a non-standard definition of g^2 .

In general, we find that the surface in our parameter space on which M^2 vanishes (in units of g^2N/a), Fig. 4, always lies above the surface of vanishing lattice string tension $a^2\sigma$; that is, the

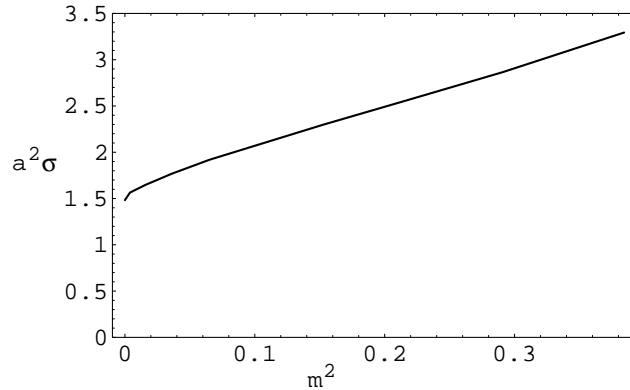


Figure 7: The lattice spacing in units of the string tension along the scaling trajectory, Table 3. Here we plot $a^2\sigma$ vs m^2 .

spectrum always becomes tachyonic before the lattice string tension vanishes. Any “critical point” must occur in the intersection of the surface of vanishing lattice string tension and vanishing mass gap. In fact, we find no such point anywhere in the $m^2 > 0$ coupling constant space, in agreement with the colour dielectric arguments of Section 2. Instead we have a scaling trajectory at finite lattice spacing, as we now show.

If we assume that our σ is equal to the ELMC value of σ , we can determine the lattice spacing a in units of the string tension along the scaling trajectory. As mentioned previously, this demonstrates that the mass $m^2 = \mu^2 a / (g^2 N)$ determines the lattice spacing and that the continuum limit occurs at $\mu^2 < 0$; see Fig. 7.

6 Density of States and T_c .

Another quantity of interest is the deconfinement temperature T_c , which on general grounds one expects to exist in a pure gauge theory in greater than 1 + 1 dimensions [24]. In the Euclidean finite temperature formalism, this is signalled by a winding mode in the Euclidean time direction which becomes tachyonic. An estimate of the inverse circumference $T = T_c$ at which this occurs comes from the formula [25] for the lowest mass eigenstate of a long closed harmonic string of winding number one:

$$M^2 = \frac{\sigma^2}{T^2} - \frac{\sigma\pi(D-2)}{3} \quad (60)$$

where D is the number of spacetime dimensions. It becomes tachyon at

$$T_c = \sqrt{\frac{3\sigma}{\pi(D-2)}} \quad (61)$$

The result $T_c \approx 0.98\sqrt{\sigma}$ for $D = 3$ is close to, but different from, that predicted by the large- N extrapolation of the ELMC results [9]:⁷ $T_c = 0.89(3)\sqrt{\sigma}$.

T_c may also be obtained from the Hagedorn behaviour [27] of the asymptotic density of mass eigenstates

$$\rho(M) \sim M^{-\alpha} \exp(M/T_c) \quad (62)$$

The canonical partition function diverges for $T > T_c$. If $\alpha > (D + 1)/2$ it is a phase transition, beyond which the canonical and microcanonical ensembles are inequivalent. If $\alpha < (D + 1)/2$ the ensembles are equivalent and T_c represents a limiting temperature — the free energy diverges at T_c . The light-cone quantisation of a free relativistic string with harmonic oscillations in the transverse direction (Nambu-Goto Bosonic string) was first performed by Goldstone *et alii* [28], who found a linearly rising discrete spectrum of squared masses

$$M^2 \sim 2\pi\sigma n, \quad n \in Z \quad (63)$$

very similar to the hadronic Regge trajectories observed in nature. Each mass level has a degeneracy increasing with n , such that the density of states ρ per unit mass yields Eqn. (61) once more. Thus large- N QCD seems to have slightly larger level density than this Bosonic string.

In the next section, we will use the density $\rho(M)$ in the LCTL formulation to understand analytically this difference between T_c in the large N gauge theory and the Bosonic string. We will discuss numerical estimates of T_c from the Hagedorn behavior in Section 6.2.

6.1 Analytic Regge Trajectories.

High mass glueballs are not quite described by the Bosonic string model. One piece of evidence for this is the discrepancy in T_c noted above. By construction, the only degrees of freedom, in addition to the centre of mass, allowed in the Bosonic string model leading to (61) are transverse oscillations. A ‘QCD string’ might also be expected to have longitudinal degrees of freedom. In fact it is well-known that allowing a relativistic string to oscillate only in transverse directions leads to consistency problems, for example with Lorentz invariance, unless $D = 26$. A correct treatment when $D \neq 26$ must allow longitudinal oscillations in an essential way [29]. Recent attempts, by one of the authors, to study directly the light-cone quantisation of such ‘non-critical’ string models have led to largely inconclusive results however [30]. The Wilson loops of our light-cone lattice dielectric theory clearly exhibit oscillations in the both the longitudinal x^- and transverse x^1 directions. We propose that the former accounts for the slight shift in T_c .

⁷The numerical ELMC result is in turn in agreement with the analytic large- N result of the Torino group for T_c based also on Euclidean lattice methods [26].

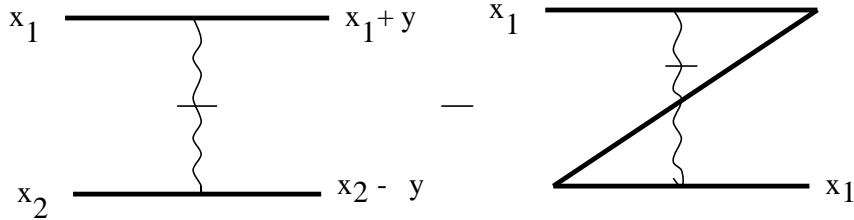


Figure 8: Coulomb exchange diagram and its self-energy contraction. Thick lines are propagating particles, wavy line the non-propagating A_+ mode.

It is instructive to derive the Hagedorn behaviour in the LCTL approach and show how the extra degrees of freedom necessary to lower T_c from its Bosonic string value might arise. The exponential density of asymptotically high mass eigenfunctions of P^- (24) derives from wavefunctions containing typically many links p , i.e. long strings. It is useful to consider two extremes of this large p problem, according to the complexity in the longitudinal dependence of the wavefunctions f on Bjorken $x = k/P^+$, conveniently measured by the typical number of nodes say. We split $P^- = P_t^- + P_l^-$ into transverse and longitudinal pieces, where from Eqn. (24)

$$P_t^- = \int dx^- V[M] \quad (64)$$

$$P_l^- = - \int dx^- \frac{g^2}{2a} \text{Tr} \left\{ J^+ \frac{1}{\partial_-^2} J^+ \right\} \quad (65)$$

There are two problems which face us now. Firstly, we expect that more terms must be added to $V[M]$ as we examine levels of higher mass in order to restore Lorentz invariance for them. Secondly, the wavefunction will not in general split into a product of longitudinal and transverse pieces. There are two extremes when one might expect a degree of universality to help.

Consider first the extreme when p takes its maximum value, for example when each link variable assumes the minimum $x = 1/K$ allowed by the DLCQ cut-off. The solutions of P^- in this limit have already been studied by Klebanov and Susskind [31] (see also Ref. [17]) in the approximation that processes which lower the number of particles are neglected.⁸ They found that for a wide range of parameters in the potential V the spectrum was precisely (63) with the correct degeneracy to produce (61). P_l^- vanishes in the approximation, so one essentially diagonalises P_t^- . They also argued that allowing some particle annihilation and creation would merely renormalise σ to a first approximation. This would mean that, as far as the asymptotically high spectrum is concerned, the purely transverse degrees of freedom of glueballs in the LCTL formulation are just those of the Bosonic string.

In the previous extreme the longitudinal dynamics were frozen by construction. Let us now

⁸We will not regurgitate the somewhat technical analysis, but refer the interested reader to the original literature.

unfreeze them by allowing oscillations in the longitudinal direction, with non-trivial dependence of the wavefunctions on Bjorken x , and go to the other extreme. The high spectrum for P_l^- typically contains wavefunctions $f_{\lambda\rho\dots\sigma}(x_1, \dots, x_p)$ which oscillate rapidly as a function of each x_i . In this case we can make the asymptotic approximation suggested by 't Hooft [18] for fundamental representation fermions in two-dimensional light-cone large- N QCD; in fact our initial analysis is only a slight modification of the corresponding one for adjoint representation fermions [32] due to Kutasov [33]. For such rapidly oscillating wavefunctions all of the terms in P_l^- tend to average to zero. The same is true of the terms in P_l^- , except for the Coulomb exchange term which is singular at zero momentum transfer ($k_2 = k_3$ in Eqn. (38)), and the creation of small- x particles from the same instantaneous A_+ mode (Eqn. (39) at $k_1 + k_2 = 0$ or $k_2 + k_3 = 0$). Keeping only the Coulomb exchange term for the moment, the P_l^- eigenvalue problem is dominated by the following part of the light-cone Schrödinger equation for the wavefunction components of a p -link state

$$M^2 f_{\lambda\rho\dots\sigma}(x_1, \dots, x_p) = \frac{g^2 N}{\pi a} \int_{-\infty}^{\infty} \frac{dy}{y^2} \{ f_{\lambda\rho\dots\sigma}(x_1, \dots, x_p) - f_{\lambda\rho\dots\sigma}(x_1 + y, x_2 - y, \dots, x_p) \} + \text{cyclic permutations} \quad (66)$$

This is obtained by projecting the Coulomb part of $P_l^- |\Psi\rangle$ onto individual Fock states. The Coulomb kernel has been simplified and the limits of the integral extended to the whole real line under the assumption that the dominant contribution comes from $y \approx 0$. The right hand side of (66) is represented by the diagrams of light-cone perturbation theory in Fig. 8. We must decide what to do about the transverse shape of the Wilson loop, represented by the indices $(\lambda, \rho, \dots, \sigma)$. In principle there will be a fine structure spectrum of transverse shapes on top of the large mass eigenvalue provided by Eqn. (66). We will make the approximation that this can be represented by an overall transverse degeneracy factor, which for simplicity we will take as the number of transverse configurations of a p -link loop $\sim 2^p$. This is an overcounting, obviously including lattice artifacts, and a more sophisticated treatment is no doubt possible. With the random distribution of transverse configurations, we can suppress the indices $(\lambda, \rho, \dots, \sigma)$ for the following; however, the number of links p remains significant. Solutions to (66) must satisfy the additional boundary conditions

$$f(x_1, x_2, \dots, x_p) = 0 \text{ if any } x_m = 0, \quad m \in \{1, \dots, p\}. \quad (67)$$

If we look for solutions symmetric under a cyclic permutation of the x_m 's, a sufficient condition for (67) is that $f(0, x_2, \dots, x_p) = 0$. The solutions are essentially those given by Kutasov [33] with minor modifications for Boson statistics. We just display the first couple:

$$f(x_1, x_2) = \sin \pi n_1 x_1; \quad M^2 = 2g^2 N \pi n_1 / a; \quad n_1 \text{ odd integer} \quad (68)$$

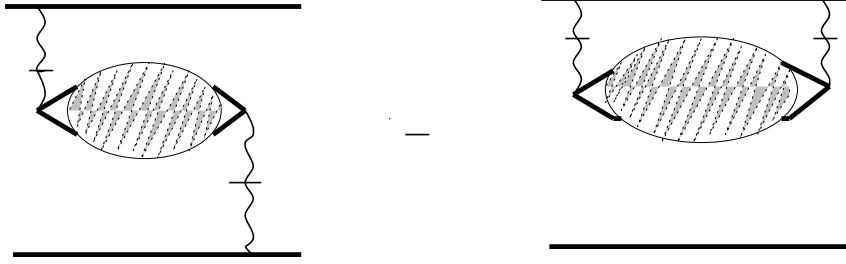


Figure 9: Self-energy corrections to the non-propagating A_+ mode. These diagrams represent dominant particle non-conserving processes when small momentum fraction y is flowing through the initial A_+ line.

$$\begin{aligned}
 f(x_1, x_2, x_3, x_4) &= \sin(\pi n_1(x_1 + x_2)) \sin(\pi n_2(x_2 + x_3)) - \sin(\pi n_1 x_1) \sin(\pi n_2 x_3) \\
 &\quad + \sin(\pi n_1 x_2) \sin(\pi n_2 x_4) + (n_1 \leftrightarrow n_2); \\
 M^2 &= 2g^2 N \pi (n_1 + n_2) / a; \quad n_1 > n_2; \quad n_i \text{ odd integers.}
 \end{aligned} \tag{69}$$

The general spectrum is

$$M^2 = \frac{2g^2 N \pi}{a} (n_1 + n_2 + \dots + n_{p/2}); \quad n_i \text{ odd.} \tag{70}$$

In general the high mass states are a mixture of different numbers of particles p , so Eqn. (66) cannot be the whole story. We must also take into account pair creation effects. The most important effect is likely to be the A_+ self-energy processes Fig. (9), which are singular when small momentum fraction y is flowing through the instantaneous A_+ line. The net effect of such “vacuum polarisation” is to give a renormalisation of the Coulomb coupling constant $g^2 N / \pi a$ and hence the mass scale setting for Eqn. (70). In fact such a renormalisation must occur since the bare expression (70) is obviously a dependent; the Coulomb exchange process cannot produce any motion on the transverse lattice. Through pair creation and annihilation of links, transverse motion becomes possible. We will not need to determine the renormalisation for the present application, since the spectrum is still of the string theory form (63) and our ignorance of the functional dependence of the mass scale on the couplings is parameterised by σ .

From the form (70) we may calculate the density of states using standard methods of statistical mechanics. The generating function

$$G(w) = \sum_n d_n w^n \tag{71}$$

defines the number of states d_n of $M^2 = 2\pi\sigma n$. For large n we need to find the behaviour as $w \rightarrow 1$. Including the transverse degeneracy factor 2^p we have explicitly

$$\log G(w) = \log \prod_{m=1}^{\infty} (1 + 4w^m)$$

$$\begin{aligned}
&= - \sum_{m,q=1}^{\infty} \frac{(-4w^m)^q}{q} \\
&= - \sum_{q=1}^{\infty} \frac{(-4w)^q}{q(1-w^q)} \\
&\sim - \frac{1}{1-w} \sum_{q=1}^{\infty} \frac{(-4)^q}{q^2} \quad (w \sim 1) \\
&= - \frac{\text{Li}_2(-4)}{(1-w)} \tag{72}
\end{aligned}$$

where Li_2 is the dilogarithm function. Then

$$d_n = \frac{1}{2\pi i} \int_{\mathcal{C}} dw \frac{G(w)}{w^{n+1}} \tag{73}$$

where \mathcal{C} encircles the origin. The integral (73) has a saddle at $\log w = \sqrt{-\text{Li}_2(-4)/n}$ giving

$$d_n = \exp \left[2\sqrt{-n\text{Li}_2(-4)} \right] \approx \exp \left[M\sqrt{\frac{4.75}{\pi\sigma}} \right] \tag{74}$$

The Hagedorn temperature $T_c = 0.81\sqrt{\sigma}$ should be regarded as a lower bound given the probable overestimate of the degeneracy of transverse configurations. The important point to note is that the density of states would rise exponentially as a result of longitudinal excitations alone, even if we did not include any degeneracy factor for transverse structure. This is strong evidence that T_c can be lower in large- N gauge theory than in free Bosonic string theory as a result of non-trivial longitudinal degrees of freedom. Our estimate, therefore, is that it lies in the range $0.81\sqrt{\sigma} < T_c < 0.98\sqrt{\sigma}$, consistent with the ELMC result.

6.2 Numerical estimates

Now we turn our attention to a numerical estimation of the density of states. For this calculation, we have only specified the box size K to truncate the basis. It is essential to demonstrate that the spectrum is sufficiently converged in K , thus we only fit to the states between $0.5 < \log(t) < 5.5$ for the $K = 7$ data; see Fig. 10. A numerical fit gives,

$$\log(t) = 3.99 + \frac{M}{0.78\sqrt{\sigma}} - 5.86 \log \left(\frac{M}{\sqrt{\sigma}} \right). \tag{75}$$

Since the density of states is $\rho(M) = dt/dM$, we find $T_c = 0.78\sqrt{\sigma}$ with an estimated error⁹ of at least 10%. Due to the large error, this result is both compatible with the Euclidean lattice result [9, 26] and the analytic bound of the previous subsection which assumed random transverse configurations. The fact that the power correction $\alpha \approx 4.86$ in the density (62) is much larger than $(D+1)/2 = 2$ means that the thermodynamic free energy remains finite at T_c , marking a true phase transition (presumably deconfinement) rather than a limiting temperature.

⁹This result could be easily improved upon since the $K = 7$ truncation contains only 4117 states.

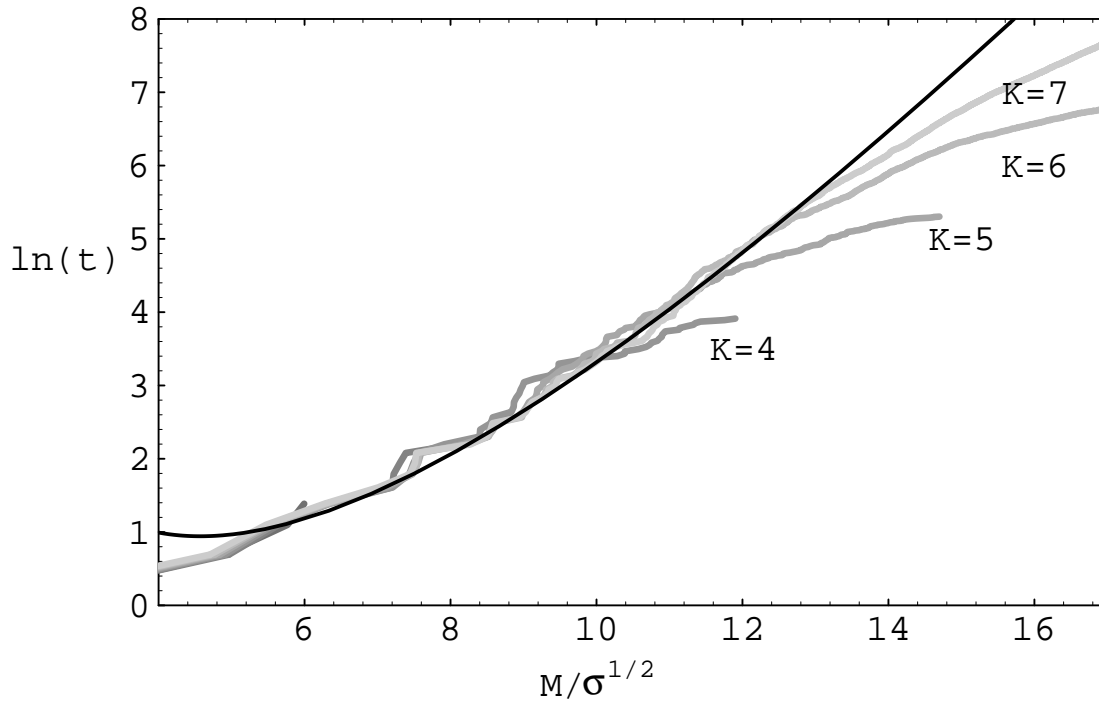


Figure 10: $\ln t$ vs the mass of the t -th eigenvalue M_t in units of the string tension. Here we have applied a cutoff in K only. Also shown is a least squares fit to the $K = 7$ data in the range $0.5 < \log(t) < 5.5$. We have chosen the couplings from the $m^2 = 0.065$ line of Table 1.

7 Conclusions

We performed light-cone quantisation of the colour dielectric lattice gauge theory on a transverse lattice, for $2 + 1$ dimensions and large N . The glueball solutions of the theory were investigated as a function of couplings in an effective potential $V[M]$ on the transverse lattice, which contained all possible gauge-invariant terms up to 4th order in M ; 4 couplings in total (plus an overall mass scale). We found an approximate scaling trajectory — a one-parameter set of couplings for which physical results are almost unchanged — along which our glueball spectrum agreed quite well with results from Euclidean lattice Monte Carlo simulations; some 18 or 19 energy levels. The surface of vanishing mass in lattice units was also found in the region of parameter space where our quantization is valid. Our scaling trajectory correctly moves towards this surface as we decrease the lattice spacing. It presumably differs from the exact scaling trajectory by higher order terms in $V[M]$ that we neglected and which represent at this stage a systematic error. However, these corrections are seen to become less important as one moves along the trajectory toward smaller lattice spacing. We also bounded and estimated the deconfinement temperature from the density of asymptotically high masses, suggesting that longitudinal string-like oscillations are responsible for deviations from the Nambu-Goto string model. Our methods in addition yield the light-cone wavefunctions for every glueball in terms of the dielectric link variables, a more detailed analysis of which will be presented in future work. We applied new numerical methods for the solution of light-cone Hamiltonians which should be useful for a range of other problems. Below we mention a couple of important questions arising from our analysis and discuss improvements and extensions to this work that we are carrying out.

7.1 Large- N phase transitions?

In lattice gauge theories with a simple action, such as the Wilson action, there is a strong crossover behaviour between strong and weak coupling which probably turns into a phase transition in the large N limit. This large N phase transition is well established in exactly solvable models [34] and is a lattice artifact, *id est* it occurs even on a single link. (Remember there are an infinite number of degrees of freedom per link at large N .) We have been tacitly assuming throughout this work that the infrared stable RG trajectory does not encounter such a large- N obstacle between the large lattice spacing regime (where the dielectric approach is valid) and the infra-red fixed point. Any truncation of the effective potential $V[M]$ almost certainly will encounter a large- N transition. This is simply illustrated by the following exactly solvable one-link theory [35]

$$Z = \int \mathcal{D}M \exp(-\mu^2 \text{Tr} \{M^\dagger M\} - \text{Tr} \{W(M^\dagger M)\}) \quad (76)$$

where $W(x) = g_2x^2 + g_3x^3 + \dots$ is a *generic* polynomial potential, with all $g_i > 0$ (this condition is convenient but not essential). Decomposing $M = U^\dagger DV$ into a real diagonal matrix D and unitary matrices U and V , the solution can be expressed entirely in terms of the distribution of eigenvalues $\rho(\lambda) d\lambda$, which is determined by a saddle point analysis at large N . Here, $\lambda > 0$ is an eigenvalue of $M^\dagger M$. For $\mu^2 > 0$ the support of $\rho(\lambda)$ is $[0, 1]$, under suitable normalisation of M , and $\rho(\lambda) \sim 1/\sqrt{\lambda}$ as $\lambda \rightarrow 0$. For sufficiently negative μ^2 the support becomes $[A, A+1]$, $A > 0$, with $\rho(\lambda) \sim \sqrt{\lambda - A}$ as $\lambda \rightarrow A$. This change in the analytic structure causes a third order phase transition in Z at a certain (negative) value of μ^2 , in direct analogy with the situation for Wilson link variables [34]. In order to avoid the phase transition, one must ensure the support exists down to $\lambda = 0$. On the other hand, according to Section 2, the effective potential should force $M^\dagger M \rightarrow 1$ as $\mu^2 \rightarrow -\infty$. These two requirements can only be met by carefully tuning a non-polynomial effective potential. The infrared stable trajectory would be of this sort. The density ρ would begin to vanish everywhere, except near $\lambda = 1$, only as the fixed point itself is reached. Any finite-order truncation of the effective potential would not leave a navigable route to the fixed point, although it may allow a trajectory at intermediate lattice spacing close to the infrared stable trajectory. It is this latter possibility that we have sought to establish in this paper.

7.2 Zero modes?

There are two sources of $k^+ = 0$ modes in the transverse lattice theory, both of which we have not used. Firstly the light-cone gauge $A_- = 0$ is not compatible with removal of the region $k^+ = 0$, although the similar gauge $\partial_- A_- = 0$ is. The difference is an extra quantum mechanical degree of freedom which will lead to a non-trivial vacuum structure in the type of theories considered here [36]. Very little is known about the quantitative effects on the spectrum. Some of the effects may just be absorbed into our effective potential. This dynamical zero mode certainly deserve further attention.

Secondly, there is the $k^+ = 0$ part of M , which we can ignore in the dielectric regime. If we decompose $M = HU$ into a ‘radial’ Hermitian matrix H and an ‘angular’ unitary matrix U , we expect that as the mass squared of the M -quanta turns negative, H gets a VEV H_0 . If $H = H_0 + \tilde{H}$, as the lattice spacing vanishes H_0 freezes while \tilde{H} becomes infinitely massive and decouples, leaving U which is nothing but the usual Wilson link variable. This is just another way of phrasing the arguments of Section 2. Evidently the Hamiltonian approach becomes very complicated once outside of the dielectric regime because of this zero mode and the necessity of decomposition into radial and angular parts. The fact that we see a slight worsening of our results at very small μ^2 may indicate that we are becoming sensitive to the onset of the above phenomenon. However we cannot rule out

that these fluctuations are due to some subtlety in the K and/or p extrapolations near $\mu^2 = 0$.

7.3 Improvements and extensions

There are two points of view one could take with regard to fixing the couplings in the effective potential $V[M]$. If one is mostly interested in determining a hadron light-cone wavefunction, an acceptable phenomenological procedure would be to tune $V[M]$ until it reproduces the mass spectrum from experiment or Euclidean lattice methods. The hadronic structure functions *et cetera* would then be predictions. We will not discuss this point of view further. Another approach is to attempt to determine the scaling trajectory *a priori* without reference to other data by examining Lorentz invariance. In this paper our only measure for this was the multiplet structure of the glueball spectrum. Although in principle one could fix $V[M]$ by demanding the correct degeneracies, in practice we found that this was not really tenable since we are working at finite lattice spacing. Indeed we found it difficult to get the lowest parity doublet to be degenerate. In addition, it takes no account of rotational invariance in the spin 0 states, which form most of light spectrum. Another method is to measure the heavy source potential in the spatial directions. In Ref. [37] this method was studied for the same light-cone Hamiltonian problem, but with $V[M]$ arbitrarily set to zero. Nevertheless, for distances greater than two lattice spacings the potential appeared remarkably rotationally invariant in (x^1, x^2) . However, over a typical hadron size (of order two or three lattice spacings according to our analysis) the results were much less satisfactory. Also, while it can test the scalar part of the interaction, it is not sensitive to the full spin dependence of the theory.

A better measure of the restoration of Lorentz invariance is provided by the relativistic dispersion relation of each glueball wavefunction which allows one to keep track of Lorentz invariance for all states, whether of zero or non-zero spin. To test whether the dispersion relation $M^2 = 2P^+P^- - (P^1)^2$ holds for each glueball requires us to work at non-zero transverse momentum P_1 . This can be done within the context of the Eguchi-Kawai reduced formulation by adding appropriate phase factors to the Hamiltonian matrix elements. It does require a certain amount of code rewriting and we plan to include this measurement in future work. It should enable us to fix an optimal effective potential for symmetry restoration and thus predict the approximate scaling trajectory without the need for a fit to an existing spectrum.

Although we have not discussed them in any detail in this paper, perhaps the most interesting output of our calculations are the light-cone wavefunctions. These may be used to calculate not only distribution functions at a given low normalisation point for the transverse momentum cutoff, but also their non-perturbative evolution as one moves along the scaling trajectory. A detailed analysis will be given in a future publication once the trajectory has been better verified.

There is the possibility of performing some sort of analytic or semi-analytic renormalisation group procedure. As we have emphasised, we cannot use small lattice spacing as a parameter to do this in the dielectric regime. However, we do have dynamical information which suggests that mixing of Fock sectors with different numbers of particles can be treated as a perturbation, and we can also use perturbation in small μ^2 if necessary. In this paper we have already performed some rudimentary analytic work to find the critical surfaces for vanishing tension and mass gap. This could probably be extended, order by order in processes which change the number of particles, to derive an approximate scaling trajectory at intermediate lattice spacing. In practice, however, it may be just as well to do this numerically. Basically we are dealing with a very discrete problem in the transverse lattice direction and numerical methods are much more efficient. In the longitudinal directions on the other hand, where we take the continuum limit, we have demonstrated that semi-analytic methods produce a vast improvement in the removal of discretisation errors.

An ‘equal-time’ Hamiltonian investigation using colour dielectric variables [2] would also be interesting as a comparison. However, even in the large N limit, the quantum vacuum becomes complicated, making study of the spectrum more difficult.

The most obvious generalization of our transverse lattice work is to $3 + 1$ dimensions [1]. The same techniques are applicable here, although the numerical computation becomes more difficult. Although one must add more terms to the effective potential to a given order in the fields, there are many more physical observables which can be used to fix the associated coupling constants.

Acknowledgements

We thank M. Burkardt, Y. Kitazawa, H-J. Pirner, and M. Teper for helpful discussions, also M. Teper for making available his ELMC results before publication. SD thanks Prof. H-C. Pauli (MPI Heidelberg) and Prof. F. Lenz (Erlangen) for hospitality during the course of the work. The work of BvdS was supported in part by the Alexander Von Humboldt Stiftung and a NATO travel grant. The work of SD was supported by the Particle Physics and Astronomy Research Council.

A Eguchi-Kawai Reduction

Large- N Eguchi-Kawai reduction at $P^1 = 0$ means that the light-cone Hamiltonian in the basis of Wilson loop Fock states built on $|0\rangle$ (30) is the same as the Hamiltonian for the corresponding problem where the transverse lattice is compactified on m links, $m \in \{1, 2, \dots\}$, *id est* one makes the identification $M_{x^1}(x^-) = M_{x^1+ma}(x^-)$ in both basis states and Hamiltonian. In particular for $m = 1$ this means the identification

$$M_{x^1}(x^-) = M(x^-) \quad \text{for all } x^1. \quad (77)$$

For the basis states themselves the identification (77) is obviously a $1 \rightarrow 1$ mapping since any single Wilson loop for a state of $P^1 = 0$ is completely specified by its shape. The shape is completely specified by the sequence of orientations of the link modes in the colour trace and does not require knowledge of the absolute positions of the modes on the lattice.

Now the original Hamiltonian (24) is quartic and local in the transverse direction. Therefore link modes on the Wilson loop interact only if they are within two lattice spacings of one another. Under reduction (77), modes which were not within two lattice spacings now lie on the same link and will interact. Also modes which were not on the same link, but were within two lattice spacings of one another, will have additional forms of interaction under reduction. The problem is to show that the extra interactions which arise from the reduction (77) are suppressed by $1/N$. This is a finite task since the Hamiltonian, being quartic, involves no more than four link modes in initial plus final states. The full proof is nevertheless quite tedious, so we illustrate the steps with a couple of examples.

Our first example is a $2 \rightarrow 2$ amplitude which occurs on neighbouring link modes before reduction. It is the combination

$$\text{Tr} \left\{ a_{+1}^\dagger(q, x^1) a_{+1}^\dagger(q', x^1 + a) a_{+1}(k', x^1 + a) a_{+1}(k, x^1) \right\}, \quad q + q' = k + k', \quad (78)$$

which comes from the operator coupling to λ_2 in the Hamiltonian

$$\frac{\lambda_2}{N} \text{Tr} \left\{ M_{x^1} M_{x^1}^\dagger M_{x^1-a}^\dagger M_{x^1-a} \right\}. \quad (79)$$

On the successive link modes

$$\text{Tr} \left\{ \dots a_{+1, kj}^\dagger(k', x^1 + a) a_{+1, ji}^\dagger(k, x^1 + a) \dots \right\} |0\rangle \quad (80)$$

the result is

$$\lambda_2 \text{Tr} \left\{ \dots a_{+1, kj}^\dagger(q', x^1 + a) a_{+1, ji}^\dagger(q, x^1) \dots \right\} |0\rangle \quad (81)$$

In the reduced theory the x^1 label is dropped in Eqns. (78), (79), and (80). The result this time is

$$\begin{aligned} & \lambda_2 \text{Tr} \left\{ \cdots a_{+1,k_j}^\dagger(q') a_{+1,j_i}^\dagger(q) \cdots \right\} |0\rangle \\ & + \frac{\lambda_2}{N} \text{Tr} \left\{ a_{+1}^\dagger(q) a_{+1}^\dagger(q') \right\} \text{Tr} \left\{ \cdots \delta_{ik} \cdots \right\} |0\rangle . \end{aligned} \quad (82)$$

The reduced amplitude picks up an extra term which is suppressed by $1/N$. Note that the longitudinal coordinate plays no role in the calculation.

Our second example is a $3 \rightarrow 1$ amplitude involving widely separated links before reduction. It is the combination

$$\text{Tr} \left\{ a_{+1}^\dagger(k_4, x^1) a_{+1}(k_1, x^1) a_{-1}(k_2, x^1) a_{+1}(k_3, x^1) \right\} , \quad k_4 = k_1 + k_2 + k_3 , \quad (83)$$

which comes from the operator coupling to λ_1 in the Hamiltonian

$$\frac{\lambda_1}{N} \text{Tr} \left\{ M_{x^1} M_{x^1}^\dagger M_{x^1} M_{x^1}^\dagger \right\} . \quad (84)$$

On the separated link modes

$$\text{Tr} \left\{ \cdots a_{+1,i_j}^\dagger(k_1, x^1) a_{-1,j_k}^\dagger(k_2, x^1) \cdots a_{+1,l_m}^\dagger(k_3, y^1) \cdots \right\} |0\rangle \quad (85)$$

the result is zero since (84) is local to the link x^1 . In the reduced case however the result is non-zero

$$\lambda_1 \text{Tr} \left\{ \delta_{kl} \cdots \right\} \text{Tr} \left\{ \cdots a_{+1,im}^\dagger(k_4) \cdots \right\} |0\rangle \quad (86)$$

Once one takes into account the N -normalisation of states, see (31), one sees that (86) is $1/N$ suppressed. The generalisation of the proof to two or more transverse dimensions is straightforward.

Eguchi-Kawai reduction was proved for Wilson's lattice gauge theory using the equivalence of the Dyson-Schwinger loop equations [10]. This equivalence required that, in the reduced formulation, extra terms proportional to the expectation value of a pair of disconnected Wilson loops with opposite non-zero winding number vanished. This was true under the assumption of large- N factorization and unbroken $U(1)$ winding number symmetry. However this $U(1)$ is spontaneously broken at weak coupling (*id est* small lattice spacing) [19], spoiling the equivalence under reduction. Our proof of equivalence in the light-cone Hamiltonian framework based on the dielectric variables in the vacuum $|0\rangle$ makes no reference to the winding sectors at all. The extra disconnected loops which give rise to the problems in the Dyson Schwinger approach have no analogue here because the large- N light-cone Hamiltonian propagates loops without splitting or joining them. This is a special feature of the light-cone quantisation which does not hold in the equal-time quantisation.

Does this mean we avoid the breakdown of Eguchi-Kawai reduction? The answer is yes, but unfortunately not in a way that that can take us to small lattice spacing. Our proof is based on the

dielectric variables acting on the vacuum $|0\rangle$. Provided this is the true vacuum, our quantisation is valid and we can use the reduced formulation. If the true vacuum lies elsewhere, which would be signalled by tachyons in the spectrum (see Fig. 4), then even our quantisation of the unreduced theory about $|0\rangle$ is not valid. In particular, our quantisation breaks down for $m^2 < 0$, which puts a lower limit on the lattice spacing we can achieve on the scaling trajectory; see Fig. 7. At present we do not know how to formulate the light-cone Hamiltonian theory in terms of variables other than the dielectric ones and, even then, anywhere other than about the $M = 0$ classical solution. Thus, even though the light-cone formulation avoids the usual source of breakdown of Eguchi-kawai reduction, we are unable to exploit this to reach small lattice spacing in the reduced theory.

B Tamm-Dancoff Extrapolation

Our numerical calculations of the glueball spectrum use a cutoff on the maximum number of link variables p in a state, *id est* a Tamm-Dancoff cutoff on the Hilbert space. Although a popular truncation scheme there is very little work in the light-cone literature on how one expects this to extrapolate to $p \rightarrow \infty$. In the following, we will use the “transverse only” model of Section 4.1 to estimate the convergence in particle truncation in the limit of large p .

Let us symmetrise our states $|\sigma_1, \dots, \sigma_p\rangle$ under orientation reversals $\mathcal{O} : \sigma_i \rightarrow \sigma_{p-i+1}$, reflections $\mathcal{P}_1 : \sigma_1 \rightarrow -\sigma_i$, and cyclic permutations. The total number of distinct states, after symmetrisation, is bounded above by $\binom{p}{p/2}$ and bounded below by $\binom{p}{p/2}/(4p)$. For large p , the actual number of distinct states should approach the lower bound because a generic many-particle state will not be symmetric under the above 3 operations. Thus, in the limit of large p the number of states is

$$\frac{2^{p-1}}{\sqrt{2\pi} p^{3/2}} \quad (87)$$

and the number of states for each value of γ is

$$\frac{2^{p+1/2-4p(\gamma-1/2)^2} \sqrt{\ln 2}}{\pi p^2} . \quad (88)$$

Note that the distribution becomes increasingly peaked at $\gamma = 1/2$ as p is increased. The normalisation for a generic state is

$$1 = \langle \sigma_1, \dots, \sigma_p | \sigma_1, \dots, \sigma_p \rangle = C_{\sigma_1, \dots, \sigma_p}^2 . \quad (89)$$

That is, we expect only one nonzero contraction for a generic many-particle state. Likewise, the number of $p - 2$ particle states that couple to a given p particle state is typically $p/2$. Assuming

only one nonzero contraction, the associated matrix element is, on average,

$$\langle \sigma_1, \dots, \sigma_p | P_\mu P^\mu | \sigma_1, \dots, \sigma_{p-2} \rangle = \frac{p(1+2\beta)\Gamma(\beta+1/2)^3\Gamma(1+4\beta)}{2\pi a\Gamma(1+2\beta)^2\Gamma(3/2+3\beta)} [2(1-\gamma)\lambda_1 + \gamma\lambda_2] (1+O(1/p)); \quad (90)$$

note that these two states must have approximately the same value of γ . Using perturbation theory, the amplitude for a generic p -particle basis state in a low energy eigenstate is

$$d_p \propto \left(\frac{p \langle \sigma_1, \dots, \sigma_p | P_\mu P^\mu | \sigma_1, \dots, \sigma_{p-2} \rangle}{2 \langle \sigma_1, \dots, \sigma_p | P_\mu P^\mu | \sigma_1, \dots, \sigma_p \rangle} \right)^{p/2} \quad (91)$$

times an undetermined power of p (which we will ignore). Again using perturbation theory, one finds for a p -particle truncation that a low energy eigenvalue converges as

$$M_p^2 - M_\infty^2 \approx -d_p^2 2p \frac{2^{p-1}}{\sqrt{2\pi} p^{3/2}} \frac{\langle \sigma_1, \dots, \sigma_p | P_\mu P^\mu | \sigma_1, \dots, \sigma_{p+2} \rangle^2}{\langle \sigma_1, \dots, \sigma_{p+2} | P_\mu P^\mu | \sigma_1, \dots, \sigma_{p+2} \rangle} \quad (92)$$

where we have estimated the number of states from Eqn. (87). Since we know from Eqn. (88) that the distribution of states is strongly peaked at $\gamma = 1/2$, we set γ to this value. (This is most valid when $2\lambda_1 \approx \lambda_2$.) Thus, the convergence in particle truncation is exponentially fast

$$M_p^2 - M_\infty^2 \propto e^{c p} \quad (93)$$

where

$$c = \ln \left| \frac{2 [\lambda_1 + \frac{\lambda_2}{2}] \Gamma(\beta + \frac{1}{2})^3 \Gamma(2\beta + 1)^2}{\Gamma(3\beta + \frac{3}{2}) \left(\left[g^2 N(1 + 4\beta) + \lambda_1 + \frac{\lambda_2}{2} \right] \Gamma(\beta + \frac{1}{2})^4 + \frac{2\pi a \mu^2 \Gamma(2\beta + 1)^4}{\beta \Gamma(4\beta + 1)} \right)} \right|. \quad (94)$$

This is the formula for convergence in particle truncation that we use in our numerical work. As illustrated in Fig. 11, it agrees well with numerical results for the ‘‘transverse only’’ model. Consequently, our biggest assumption is that it can be applied to the full theory as well.

C Improved matrix elements for DLCQ

In this section, we will describe a novel technique for improving the numerical convergence of calculations which employ Discretised Light Cone Quantisation (DLCQ) [38] to solve the associated set of coupled integral equations. An important advantage of DLCQ in a many particle calculation is that the resulting Hamiltonian matrix is quite sparse and it is essential that we preserve this property when making any improvements.

The integer-valued ‘‘harmonic resolution’’ K denotes the coarseness of the longitudinal momentum discretisation. Naïvely, one would expect that the leading finite K error associated with a DLCQ calculation would go as $1/K^2$; this is simply the error associated with approximating an

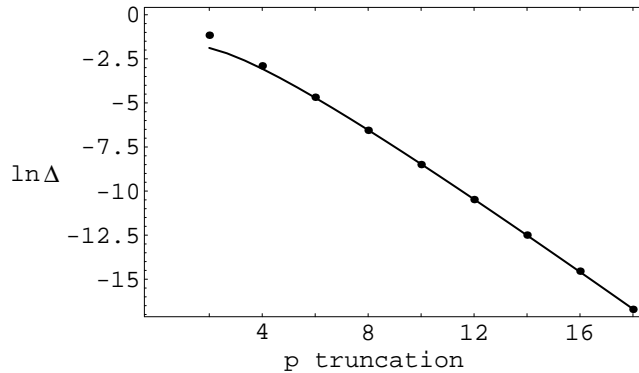


Figure 11: Convergence of eigenvalues $\ln \Delta = \ln |M_p^2 - M_\infty^2|$ vs particle truncation p for the “transverse only” model. Here, we have chosen $\mu^2 = 0$, $\lambda_1 = -0.1g^2N$, and $\lambda_2 = -0.2g^2N$. The points are from a numerical calculation using the basis (43). Also shown is a numerical fit to the function $-0.698 + cp + 1.597 \ln p$ where $c = -1.145$ is given by Eqn. (94).

integral using the trapezoidal rule. However, our Hamiltonian contains several singularities which make the convergence substantially slower. First, there are (integrable) endpoint singularities which go as $1/\sqrt{k^+}$ and produce a leading error of $1/\sqrt{K}$. Second, there is the (non-integrable) singularity associated with the mass term and the instantaneous interaction $1/(k^+ - p^+)^2$ which gives a leading error of $1/K^{2\beta}$ [39]. Finally, the error for producing a state with more particles goes as $1/\sqrt{K}$.

Our method is the following: when calculating the matrix elements of the Hamiltonian in a many-particle calculation, we will use ordinary DLCQ commutation relations to calculate contractions associated with spectator particles. To calculate the interaction itself, we take the DLCQ momenta of the interacting particles, project onto a smooth wavefunction basis (continuous longitudinal momentum), and calculate matrix elements of the interaction in this smooth wavefunction basis. Our modification of DLCQ essentially eliminates the $1/\sqrt{K}$ and $1/K^{2\beta}$ errors mentioned above. The remaining errors include a (small) $1/K$ error from the instantaneous interaction $1/(k^+ - p^+)^2$, $1/K^2$ errors from DLCQ itself, and a $1/K$ error from production of particles at small momentum.

We will discuss the (2 particles) \rightarrow (2 particles) and the (1 particle) \rightarrow (3 particles) interactions separately since we use somewhat different techniques for each.

C.1 (2 particles) \rightarrow (2 particles) interactions

Consider a typical 4-point interaction

$$V\left(\frac{k_1}{K}, \frac{k_3}{K}\right) = \text{Diagram} \quad (95)$$

with longitudinal momenta $k_i \in \{1/2, 3/2, \dots\}$ and $K = k_1 + k_2 = k_3 + k_4$. We start by calculating the first K eigenstates of the two-particle bound state equation [1]

$$\begin{aligned} M^2 \Psi(x) &= \int_0^1 dy H(x, y) \Psi(y) \\ &= \frac{\mu^2 \Psi(x)}{x(1-x)} - \frac{g^2 N}{2\pi a} \int_0^1 dy \frac{\Psi(y)}{\sqrt{x(1-x)y(1-y)}} \left(\frac{(x+y)(2-x-y)}{(x-y)^2} + 1 \right) \end{aligned} \quad (96)$$

where a principal value prescription is assumed for the integral. Here, we have chosen $2\lambda_1 + \lambda_2 + 2\lambda_3 = -g^2 N$ so that, at $\mu^2 = 0$, the lowest wavefunction is constant with eigenvalue zero. Then we write the incoming and outgoing DLCQ states as linear combinations of these K eigenfunctions and evaluate matrix elements of the interaction $V(x, y)$ in the eigenfunction basis. The result is expressed as a Taylor expansion in β . Details are described in the following.

We introduce a basis of even and odd polynomial wavefunctions (labeled by subscripts s and s'):

$$\phi_s(x) = (x(1-x))^{\beta+s-1} \begin{cases} 1 \\ 1-2x \end{cases}, \quad (97)$$

$s \in \{1, 2, \dots, S\}$, $S \gg K/2$, and β was defined in Eqn. (41). We define, for both even and odd wavefunctions, matrix elements of the interaction term $V_{s,s'} = \int dx dy \phi_s(x) V(x, y) \phi_{s'}(y)$, the inner product matrix $E_{s,s'} = \int dx dy \phi_s(x) \phi_{s'}(y)$, and the two-particle Hamiltonian (96) $H_{s,s'} = \int dx dy \phi_s(x) H(x, y) \phi_{s'}(y)$. We can Taylor expand these matrices in powers of β : $V_{s,s'} = V_{s,s'}^{(0)} + \beta V_{s,s'}^{(1)} + \dots$, $E_{s,s'} = E_{s,s'}^{(0)} + \beta E_{s,s'}^{(1)} + \dots$, and $H_{s,s'} = H_{s,s'}^{(0)} + \beta H_{s,s'}^{(1)} + \dots$. Using the formulas in Refs. [1, 40] along with the definition of the Beta function $B(\alpha, \beta) = \int_0^1 dx x^{\alpha-1} (1-x)^{\beta-1}$, $V_{s,s'}^{(n)}$, $E_{s,s'}^{(n)}$, and $H_{s,s'}^{(n)}$ can be determined analytically. In addition, we define a $K \times S$ matrix $T_{i,s}$ which maps the wavefunction basis onto the DLCQ basis (the subscript $i \in \{1, 2, \dots, K\}$ denotes a two particle DLCQ basis state with momenta $k_1 = i - 1/2$, $k_2 = K - k_1$)

$$T_{i,s} = T_{i,s}^{(0)} + \beta T_{i,s}^{(1)} + \dots = \left(\frac{k_1 k_2}{K^2} \right)^{\beta+s-1} \begin{cases} 1 \\ \frac{k_1 - k_2}{K} \end{cases}. \quad (98)$$

However, the polynomial basis that we introduced has a fatal flaw: the inner product matrix $E_{s,s'}$ is very poorly conditioned [41]. Instead, we find a new, well-conditioned, basis (denoted by subscripts ν , ρ , and σ) in which $E^{(0)}$ is diagonal. Thus, for both even and odd wavefunctions, we define the Cholesky decomposition [41]¹⁰ $E^{(0)} = LL^T$ and calculate the matrix products

$$V_{\nu,\rho}^{(n)} = (L^{-1})_{\nu,s} V_{s,s'}^{(n)} (L^{-T})_{s',\rho}, \quad (99)$$

$$E_{\nu,\rho}^{(n)} = (L^{-1})_{\nu,s} E_{s,s'}^{(n)} (L^{-T})_{s',\rho}, \quad (100)$$

$$H_{\nu,\rho}^{(n)} = (L^{-1})_{\nu,s} H_{s,s'}^{(n)} (L^{-T})_{s',\rho}, \quad (101)$$

$$T_{i,\nu}^{(n)} = T_{i,s}^{(n)} (L^{-T})_{s,\nu}. \quad (102)$$

¹⁰ The matrix elements of the lower triangular matrix L^{-1} are related to the coefficients of the Legendre polynomials defined on the interval [0,1].

Because the polynomial basis is poorly conditioned, all of the above calculations, including the matrix products (99) – (102), are numerically unstable and must be performed either exactly or using high precision arithmetic.

Working in the well-conditioned basis, we solve generalised eigenvalue problem $H\chi_t = h_t E\chi_t$ with eigenvalues $h_t = h_t^{(0)} + \beta h_t^{(1)} + \dots$ and eigenvectors $\chi_t = \chi_t^{(0)} + \beta \chi_t^{(1)} + \dots$. First, we solve the leading order eigenvalue problem $H^{(0)}\chi_t^{(0)} = h_t^{(0)}\chi_t^{(0)}$ (recall $E_{\nu,\rho}^{(0)}$ is the identity). Nonleading powers in β are calculated using Rayleigh-Schrödinger perturbation theory extended to the generalised eigenvalue problem. Thus, if we write

$$\chi_t = \chi_t^{(0)} + \beta \sum_u c_{t,u}^{(1)} \chi_u^{(0)} + \dots \quad (103)$$

then

$$h_t^{(1)} = \chi_t^{(0)\dagger} \left(H^{(1)} - h_t^{(0)} E^{(1)} \right) \chi_t^{(0)} \quad (104)$$

$$c_{t,u}^{(1)} = \frac{\chi_u^{(0)\dagger} \left(H^{(1)} - h_t^{(0)} E^{(1)} \right) \chi_t^{(0)}}{h_t^{(0)} - h_u^{(0)}}, \quad t \neq u \quad (105)$$

$$c_{t,t}^{(1)} = -\frac{1}{2} \chi_t^{(0)\dagger} E^{(1)} \chi_t^{(0)} \quad (106)$$

\vdots

Using the lowest K eigenvectors, χ_t , we define an eigenstate basis (denoted by subscripts t and t'),

$$T_{i,t} = T_{i,\nu} (\chi_t)_\nu. \quad (107)$$

The matrix $T_{i,t}$ maps the eigenfunction basis onto the DLCQ basis and $T_{i,t} T_{t,j}$ is nearly equal to the identity. In order that the map between the eigenfunction basis and the DLCQ basis preserves eigenvalues, we find an orthonormal matrix that is nearly equal to $T_{i,t}$. Thus, we perform a standard QR-factorisation [41]¹¹ $T = QR^T$ where $Q = Q^{(0)} + \beta Q^{(1)} + \dots$ is orthogonal and $R^T = R^{(0)T} + \beta R^{(1)T} + \dots$ is upper triangular. To obtain non-leading orders in β , we use the relation

$$Q^{(0)T} Q^{(n)} + R^{(n)T} R^{(0)-T} = Q^{(0)T} \left(T^{(n)} - \sum_{m=1}^{n-1} Q^{(m)} R^{(n-m)T} \right) R^{(0)-T} \quad (108)$$

and the orthonormality condition

$$Q^{(n)T} Q^{(0)} + Q^{(0)T} Q^{(n)} = - \sum_{m=1}^{n-1} Q^{(m)T} Q^{(n-m)}. \quad (109)$$

Eqn. (109) determines the diagonal matrix elements of $Q^{(0)T} Q^{(n)}$. We can use (108) to determine the strictly lower triangle of $Q^{(0)T} Q^{(n)}$ and then we use (109) to determine the upper triangle of

¹¹That is, Gram-Schmidt orthogonalisation.

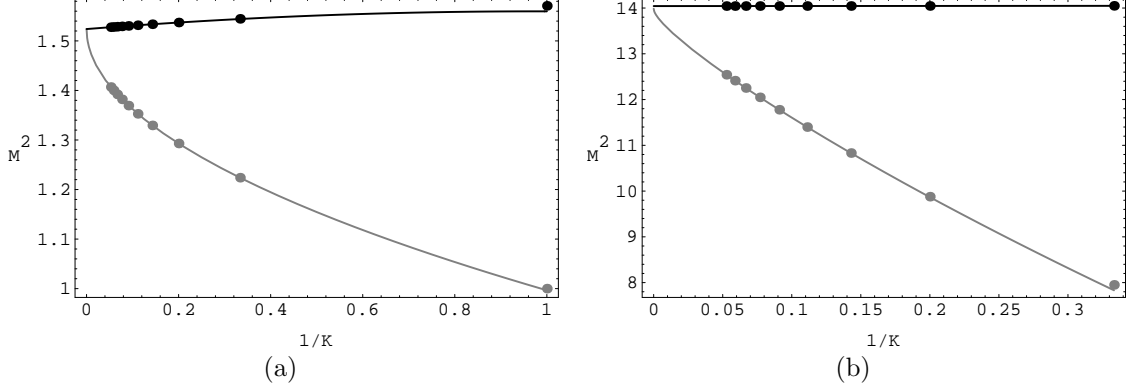


Figure 12: Convergence of the (a) ground and (b) second excited states vs $1/K$, two particle truncation, $\lambda_1 = \lambda_2 = \lambda_3 = 0$ for $\mu^2 = 0$. The grey points are from standard DLCQ and the black points are from using the improved matrix elements. In (b), the eigenvalue for the improved matrix elements is $M^2 \approx 14.043 + 0.012/K + 0.0085/K^2$.

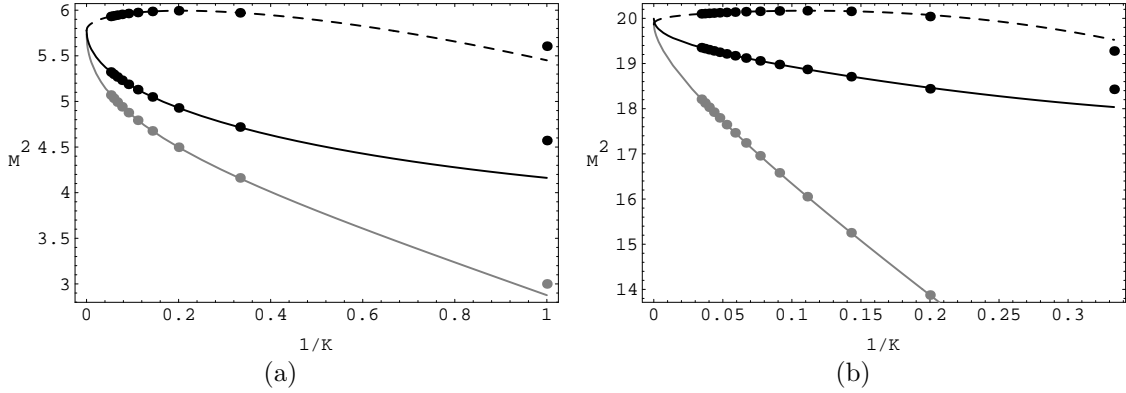


Figure 13: Convergence of the (a) ground and (b) second excited states vs $1/K$, two particle truncation, $\lambda_1 = \lambda_2 = \lambda_3 = 0$ for $\mu^2 = g^2 N / (2a)$ or $\beta = 1/4$. The grey points are from standard DLCQ, the black line is with the improved matrix elements expanded to order β^0 , and the dashed line is with the improved matrix elements expanded to order β^1 .

$Q^{(0)T} Q^{(n)}$. Finally, we use (108) to determine $R^{(n)T} R^{(0)-T}$. From this, we can determine $Q^{(n)}$ and $R^{(n)T}$.

We discard R^T and use Q to rotate to the DLCQ basis,

$$V_{i,j} = Q_{i,t} (\chi_t)_\nu^\dagger V_{\nu,\rho} (\chi_{t'})_\rho Q_{t',j}^T. \quad (110)$$

$V_{i,j}$ can be calculated order-by-order in β . To see how well the improved matrix elements work, we can look at the eigenvalues vs K for a two particle truncation. The convergence with K for $\mu^2 = 0$ and $\mu^2 = g^2 N / (2a)$ is shown in Figs. 12 and 13.

Even though the mass term is a two-point interaction, we calculate its matrix elements as if it were a four-point interaction. Note that the expansion of the mass term in powers of β , has an order $1/\beta$ contribution.

In the (2 particles) \rightarrow (2 particles) case, we use $S = 40$ states in our polynomial wavefunction basis; calculations in this basis were performed with Mathematica using exact arithmetic (except for $T_{i,s}$ where high-precision floating point arithmetic was used). For, the (1 particle) \rightarrow (3 particles) calculations, we used standard numerical techniques to perform the associated integrations.

In practice, we calculate matrix elements of the various interaction terms beforehand and store them in a file. In a many-particle calculation, the computer program simply looks up the appropriate matrix element in a table [42].

References

- [1] W. A. Bardeen and R. B. Pearson, Phys. Rev. D **14**, 547 (1976);
W. A. Bardeen, R. B. Pearson, and E. Rabinovici, Phys. Rev. D **21**, 1037 (1980).
- [2] G. Mack, Nucl. Phys. **B235**, 197 (1984).
- [3] H. B. Nielsen and A. Patkos, Nucl. Phys. **B195**, 137 (1982).
- [4] J. B. Kogut and L. Susskind, Phys. Rev. D **9**, 3501 (1974).
- [5] T. D. Lee, *Particle Physics and Introduction to Field Theory*, Harwood, Chur (1981).
- [6] S. L. Adler, Rev. Mod. Phys. **56**, 1 (1984).
- [7] H.-J. Pirner, Prog. Part. Nucl. Phys. **29**, 33 (1992).
- [8] K. G. Wilson, Phys. Rev. D **10**, 2445 (1974).
- [9] M. Teper, Phys. Lett. B **289**, 115 (1992); Phys. Lett. B **311**, 223 (1993); Nucl. Phys. (Proc. Suppl.)**53**, 715 (1997); Oxford University Report OUTP-97-01P (unpublished) [[hep-lat/9701004](#)].
- [10] T. Eguchi and H. Kawai, Phys. Rev. Lett. **48**, 1063 (1983).
- [11] S. Dalley and B. van de Sande, Nucl. Phys. **B53** (Proc. Suppl.), 827 (1997), [[hep-ph/9602291](#)];
B. van de Sande and S. Dalley, in *Neutrino Mass, Dark Matter, Gravitational Waves, Monopole Condensation, and Light Cone Quantization*, eds. C.B.N. Kursunoglu *et al.*, (Plenum Press, New York, 1996), pp. 223–240, [[hep-ph/9604268](#)].
- [12] K. G. Wilson, in *Recent Developments of Gauge Theories*, eds. G. 't Hooft *et alia*. Plenum, New York (1980).
- [13] E. Brézin and D. J. Gross, Phys. Lett. B **97**, 120 (1980).
- [14] F. Niedermayer, Nucl. Phys. **B53** (Proc. Suppl.), 56 (1997).
- [15] M. Creutz, Phys. Rev. Lett. **45**, 313 (1979).
- [16] J. B. Kogut and L. Susskind, Phys. Rev. D **11**, 395 (1975).
- [17] S. Dalley and T. R. Morris, Int. Journal Mod. Phys. **A5**, 3929 (1990).
- [18] G. 't Hooft, Nucl. Phys. **B72**, 461 (1974).

- [19] G. Bhanot, U. M. Heller, and H. Neuberger, Phys. Lett. B **113**, 47 (1982);
A. Gonzalez-Arroyo and M. Okawa, Phys. Lett. B **120**, 174 (1983).
- [20] F. Antonuccio and S. Dalley, Nucl. Phys. B **461**, 275 (1996).
- [21] B. van de Sande and M. Burkardt, Phys. Rev. D **53**, 4628 (1996).
- [22] K. Hornbostel, Ph. D Thesis, SLAC-PUB No. 333 (1988).
- [23] M. Lüscher, Nucl. Phys. **B180**, 317 (1981);
P. de Forcrand, G. Schierholz, H. Schneider, M. Teper, Phys. Lett. B **160**, 137 (1985).
- [24] B. Svetitsky, Phys. Rep. **132**, 1 (1986).
- [25] O. Alvarez, Phys. Rev. D **24** (1981) 440;
P. Olesen, Phys. Lett. B **160**, 405 (1985).
- [26] M. Billo, M. Caselle, A. D'Adda, and S. Panzeri, Int. J. Mod. Phys. A **12**, 1783 (1997).
- [27] R. Hagedorn, Nuovo Cimento Suppl. **3**, 147 (1965);
S. Frautchi, Phys. Rev. D **3**, 2821 (1971);
R. D. Carlitz, Phys. Rev. D **5**, 3231 (1972).
- [28] P. Goddard, J. Goldstone, C. Rebbi, and C. Thorn, Nucl. Phys. **B56**, 109 (1973).
- [29] A. M. Polyakov, Phys. Lett. B **103**, 207 (1981).
- [30] S. Dalley and I. R. Klebanov, Phys. Lett. B **298**, 79 (1993);
K. Demeterfi and I. R. Klebanov, Lecture by IRK at 7th Nishinomiya-Yukawa Memorial Symposium Quantum Gravity, Japan 1992, [[hep-th/9301006](#)];
S. Dalley, in *Quantum Field Theory and String Theory*, eds. L. Baulieu *et al.*, Plenum (1995), pp.71–80;
S. Dalley, Phys. Lett. B **334**, 61 (1994);
F. Antonuccio and S. Dalley, Phys. Lett. B **348**, 55 (1995).
- [31] I. R. Klebanov and L. Susskind, Nucl. Phys. **B309**, 175 (1988).
- [32] S. Dalley and I. R. Klebanov, Phys. Rev. D **47**, 2517 (1993).
- [33] D. Kutasov, Nucl. Phys. **B414**, 33 (1994).
- [34] D. J. Gross and E. Witten, Phys. Rev. D **21**, 446 (1980).

- [35] S. Dalley, C. V. Johnson, and T. R. Morris, Nucl. Phys. **B368**, 625 (1992).
- [36] H.-C. Pauli, A. C. Kalloniatis, and S. Pinsky, Phys. Rev. D **52**, 1176 (1995).
- [37] M. Burkardt and B. Klindworth, Phys. Rev. D **55**, 1001 (1997).
- [38] H.-C. Pauli and S. J. Brodsky, Phys. Rev. D **32**, 1993 and 2001 (1985).
- [39] B. van de Sande, Phys. Rev. D **54**, 6347 (1996).
- [40] K. Harada, T. Sugihara, M. Taniguchi, and M. Yahiro, Phys. Rev. D **49**, 4226 (1994).
K. Harada, A. Okazaki, M. Taniguchi, Phys. Rev. D **54**, 7656 (1996).
- [41] W. H. Press, B. P. Flannery, S. A. Teukolsky, and W. T. Vetterling, *Numerical Recipes*, Cambridge University Press (1989);
G. H. Golub and C. F. Van Loan, *Matrix Computations*, Johns Hopkins University Press (1983).
- [42] The data files and instructions for use are available on World Wide Web at <http://theorie3.physik.uni-erlangen.de/~bvds/info.html>.